

# **Final Report on 2002 Testing of Airborne Vertical Magnetic Gradiometer System**

**ESTCP Projects 200037 and 37**

**Revision 1**

**Prepared by**

**Environmental Sciences Division  
Oak Ridge National Laboratory**

**August, 2005**



**Environmental Security  
Technology Certification  
Program**



# Table of Contents

Table of Contents .....	i
Acronym List .....	iii
List of Figures .....	iv
List of Tables .....	vii
Acknowledgements .....	viii
Abstract .....	ix
1 Introduction .....	1
1.1 Background .....	1
1.2 Objectives of the Demonstration .....	2
1.3 Regulatory Drivers .....	2
1.4 Stakeholder / Enduser Issues .....	2
2 Technology Description .....	3
2.1 Technology Development and Application .....	3
2.2 Previous Testing of the Technology .....	3
2.3 Factor Affecting Cost and Performance .....	4
2.4 Advantages and Limitations of the Technology .....	4
3 Demonstration Design .....	5
3.1 Performance Objectives .....	5
3.2 Selecting Test Sites .....	5
3.3 Test Site History / Characteristics .....	6
3.4 Present Operations .....	9
3.5 Pre-demonstration Testing and Analysis .....	9
3.6 Testing and Evaluation Plan .....	10
3.6.1 Demonstration Set-up and Start-up .....	10
3.6.2 Period of Operations .....	10
3.6.3 Area Characterized .....	10
3.6.4 Residuals Handling .....	10
3.6.5 Operating Parameters for the Technology .....	11
3.6.6 Experimental Design .....	11
3.6.7 Sampling Plan .....	15
3.6.8 Demobilization .....	15
4 Performance Assessment .....	16
4.1 Performance Criteria .....	16
4.2 Performance Confirmation Methods .....	17
4.3 Data Analysis, Interpretation and Evaluation .....	19
4.3.1 Aerodynamic Stability .....	19
4.3.2 Rotor Noise .....	19
4.3.3 Maneuver Noise .....	24
4.3.4 Altitude and Positioning Errors .....	27
4.3.5 Delineation of Clustered Targets .....	29
4.3.6 Increased Altitude .....	32
4.3.7 Horizontal Gradients .....	34

4.3.8	Field Results.....	37
	Field Results – Laguna.....	37
	Field Results – APG.....	43
	Field Results – BBR.....	52
4.3.9	Recommendations for design modifications.....	59
5	Cost Assessment .....	62
5.1	Cost Reporting .....	62
6	Implementation Issues .....	69
6.1	Environmental Checklist.....	69
6.2	Other Regulatory Issues.....	69
6.3	End-User Issues .....	69
7	References.....	70
8	Points of Contact.....	71
Appendix A: Analytical Methods Supporting the Experimental Design.....		72
Appendix B: Analytical Methods Supporting the Sampling Plan .....		72
Appendix C: Quality Assurance Project Plan (QAPP).....		73
Appendix D: Health and Safety Plan .....		74
Appendix E: Dig list for APG from vertical gradient data .....		78

## Acronym List

AGL	Above ground level
AS	Analytic signal
ASCII	American Standard Code for Information Interchange
ADU	Attitude determination unit
APG	Aberdeen Proving Ground
BBR	Badlands Bombing Range, South Dakota
CERCLA	Comprehensive Environmental Response, Compensation, and Liability Act
DAS	Data analysis system
DoD	Department of Defense
DQO	Data Quality Objective
ESTCP	Environmental Security Technology Certification Program
FAA	Federal Aviation Administration
FOM	Figure of Merit
FUDS	Formerly Used Defense Sites
GIS	Geographic Information System
GPS, DGPS	(Differential) Global Positioning System
HAZWOPR	Hazardous Waste Operations and Emergency Response
HG	Horizontal (magnetic) gradient
INS	U.S. Immigration and Naturalization Service
IR	Improvement Ratio
MTADS	Multi-Sensor Towed Array Detection System
NAD	North American Datum
ORAGS	Oak Ridge Airborne Geophysical System
ORNL	Oak Ridge National Laboratory
SERDP	Strategic Environmental Research & Development Program
STC	Supplemental Type Certificate
TIF, GeoTIF	(Geographically referenced) Tagged Information File
TF	Total (magnetic) field
USAESCH	U.S. Army Engineering and Support Center, Huntsville
UTM	Universal Transverse Mercator
UXO	Unexploded Ordnance
VG	Vertical (magnetic) gradient

## List of Figures

Figure 2-1: Photos of (a) ORAGS-Arrowhead total field magnetometer system and (b) ORAGS-VG vertical magnetic gradient system with 1m vertical and 1m horizontal sensor offsets.....	3
Figure 3-1: Aerial photo of BBR Bombing Target 1.....	6
Figure 3-2: Photo of central debris mound at Laguna N-10 bombing target.....	7
Figure 3-3: Airphoto showing calibration grid (checkout) and Airfield (open field) sites at Aberdeen Proving Ground. ....	8
Figure 4-1: Time series of total field magnetic response illustrating helicopter rotor noise. ....	20
Figure 4-2: High frequency total field magnetic noise distribution about a helicopter. Dots show location of sensors from ORAGS-Hammerhead configuration. Lateral sensor locations correspond to 2.6m, 4.3m and 6.0m from helicopter centerline. ...	20
Figure 4-3: High frequency total field and vertical gradient noise vs distance from centerline of helicopter. ....	21
Figure 4-4: High frequency vertical gradient measurements at various locations along the lateral boom. ....	21
Figure 4-5: Power spectrum of total field and vertical gradient data while airborne. ....	22
Figure 4-6: Profiles over three small UXO targets. Note coherent total field noise between upper and lower sensors at arrows, and subsequent attenuation in vertical gradient. Targets are 60mm illumination rounds, average height of lower sensor is 0.9m. ....	22
Figure 4-7: Sample of total field and vertical gradient maneuver noise. Comparison of the top two panels (raw TF to raw VG) illustrates the improved FOM of the vertical gradient. Comparison of the top and bottom panels (raw to comp for both TF and VG) illustrates the consistency of the IR. ....	25
Figure 4-8: First order analytic signal derived from (a) total field (lower sensor) and from (b) vertical gradient data over a calibration grid. Horizontal units in meters, average height of lower sensor 0.9m. Black line represents path of profile from Figure 4-6. Line-line deflections in the total field-based results demonstrate uncompensated maneuver noise accentuated by grid splining. ....	26
Figure 4-9: Power spectra of the total field and vertical gradient signature of a dipole..	29
Figure 4-10: Calculated total field for a horizontal dipole at 1m depth with upper and lower magnetometers at 1.5m and 2.5m AGL, and the resulting measured vertical gradient. ....	30
Figure 4-11: Extract of analytic signal over Cuny Table Bombing Target 1. Data are derived from (a) lower sensor total field and (b) measured vertical gradient.....	31
Figure 4-12: Peak response vs depth for a simple dipole. The numeric equivalence of nT and nT/m for a narrow band of low altitudes is demonstrated. Representative noise levels with a 5:1 advantage in signal-noise for the vertical gradient show a 1.5m height advantage. ....	32

Figure 4-13: Laguna Test Grid analytic signal derived from lower sensor total field (left side) and from vertical gradient (right side) at various heights. Color coded arrows indicate anomalies on the threshold of detection. Solid arrows would be above the threshold, hollow arrows would be below the threshold. .... 33

Figure 4-14: Contour maps of total field (top-left), vertical gradient (top-rt), transverse horizontal gradient (bot-left) and longitudinal horizontal gradient (bot-rt). Same data set as Figure 4-8 and the profile from Figure 4-6. Note the reduction of maneuver noise from the original total field, to calculated longitudinal gradient, measured horizontal gradient and measured vertical gradient (highest to lowest noise). Horizontal units in meters. .... 35

Figure 4-15: Comparison of analytic signal maps derived from calculated vs measured horizontal gradients. Measured vertical gradient (vg-meas) is combined with FFT grid-calculated horizontal gradients to produce one version of the analytic signal (as-vg). It is also combined with the measured horizontal gradients to produce a second version of the analytic signal (as-meas). The noise reduction inherent in the horizontal gradients is better than that in the total field, but not enough to create a better analytic signal map. .... 36

Figure 4-16: Comparison of vertical gradient data at the Laguna test grid for the (a) 1m and (b) 0.5m vertical sensor separations. Horizontal separations were 1m and lines were interleaved. The 1m vertical separation showed slightly higher noise levels due to excessive pod vibration. .... 39

Figure 4-17: Analytic signal map over N-10 bombing target derived from (a) the lower sensor total field data and (b) the vertical gradient data. .... 40

Figure 4-18: Extract of analytic signal map over N-10 bombing target derived from (a) the lower sensor total field data and (b) the vertical gradient data. Background levels adjacent to the strong response of the central target are slightly elevated by the FFT integral calculations. .... 41

Figure 4-19: Analytic Signal at the Grenade Range derived from the 0.5m vertical gradient data. .... 42

Figure 4-20: ROC curve from APG Calibration Grid using the final automated picking and discrimination routines applied to the vertical gradient data. .... 45

Figure 4-21: ROC curve from APG Airfield using the final automated picking and discrimination routines applied to the vertical gradient data. .... 45

Figure 4-22: Vertical Gradient map over the APG Calibration Grid. Seeded items are presented as circles, picked anomalies as numbered crosses. .... 47

Figure 4-23: Analytic Signal map over the APG Calibration Grid derived from the vertical gradient. Seeded items are presented as circles, picked anomalies as numbered crosses. .... 48

Figure 4-24: Vertical gradient map of the APG Airfield site. .... 49

Figure 4-25: Analytic Signal derived from the vertical gradient at the APG Airfield site. .... 50

Figure 4-26: Vertical gradient map of a section of the APG Mine, Grenade, Direct-fire Weapon Range. .... 51

Figure 4-27: Vertical gradient response over the BBR Test Grid. Survey parameters included 1m survey height with 1m vertical sensor separation and 1m horizontal sensor separation..... 54

Figure 4-28: Analytic signal response over the BBR Test Grid as derived from the vertical gradient data in Figure 4-27..... 55

Figure 4-29: BBR Test Grid data from (a, b) 3m and (c, d) 5m survey altitudes. The wavy noise in the grids are the result of spatially-coherent low-amplitude remnants of rotor noise which is now visible with the finer color contours. .... 56

Figure 4-30: Vertical gradient response over Bombing Target 1. Survey parameters include 1.5m survey height, 1m vertical sensor separation, 1m horizontal separation. .... 57

Figure 4-31: Analytic signal response over Bombing Target 1 derived from vertical gradient data in Figure 4-30..... 58

Figure 4-32: Extract of analytic signal data from BBR Test Grid at 1m survey altitude (25m reference grid, color scale as per original Figure 4-28). (a) original 1m line spacing (b) odd number lines to represent 2m line spacing (c) even number lines. Note how small targets may be lost with inadequate line spacing. .... 60

Figure 4-33: Extract of analytic signal data from BBR Test Grid at 3m survey altitude (25m reference grid, color scale as per original Figure 4-29). (a) original 1m line spacing (b) odd number lines to represent 2m line spacing (c) even number lines. Even though very small targets are below the detection threshold, those that are detectable are broad enough to be detected at the wider line spacing. .... 60

## List of Tables

Table 3-1: Performance objectives of vertical gradient system.....	5
Table 3-2: Sensor noise measured as standard deviation of the signal for different horizontal sensor spacing. Vertical spacing less than 20cm is not possible due to the physical dimensions of the sensors.....	9
Table 3-3: Period of operations for vertical gradient system tests.....	10
Table 3-4: Size of areas characterized in hectares.....	10
Table 3-5: Locations of GPS base station monuments.....	12
Table 4-1: Performance Criteria .....	16
Table 4-2: Expected performance and performance confirmation method .....	18
Table 4-3: Calculation of signal-noise ratios for total field (TF), vertical gradient (VG), horizontal transverse gradient (HG) and horizontal longitudinal gradient (LG), based on the three anomalies shown in Figure 4-6.....	23
Table 4-4: Laguna Calibration Site seed items including the eight inert ordnance casings (or pieces of ordnance) and two iron stakes.....	38
Table 4-5: Pd and FP for various detection and discrimination techniques applied to the Airfield site at Aberdeen Proving Ground. UV indicates univariate discrimination, MV is multivariate, and DAS is the MTADS-DAS manual selection method applied to the TF data.....	44
Table 4-6: Pick list from APG calibration grid using ORAGS-VG data. XY are in local coordinate projection in meters, AS is analytic signal peak in nT/m. ID numbers correspond to the numbers shown on maps in Figures 4-22 and 4-23.....	46
Table 4-7: Items buried at the BBR Calibration Site.....	53
Table 8-1: Points of Contact .....	71

## **Acknowledgements**

This work was funded by the Environmental Security Technology Certification Program under the direction of Dr. Jeffrey Marqusee and Dr. Anne Andrews, and supported by Mr. Scott Millhouse at the U.S. Army Corps of Engineers Mandatory Center of Excellence for Ordnance and Explosives, Huntsville, Alabama. The report was written by employees of Oak Ridge National Laboratory. Oak Ridge National Laboratory is managed by UT-Battelle, LLC for the U.S. Department of Energy under contract DE-AC05-00OR22725. A contractor of the U. S. Government has authored the submitted manuscript. Accordingly, the U.S. Government retains a nonexclusive, royalty-free license to publish or reproduce the published form of this contribution, or allow others to do so, for U. S. Government purposes. We thank the Laguna Nation, the Oglala Sioux Nation, and Aberdeen Proving Ground support staff for allowing access to the various sites on their land.

## **Abstract**

Tests of a prototype airborne vertical magnetic gradiometer system were conducted at three sites in 2002 – Pueblo of Laguna NM, Aberdeen Proving Ground MD, and Badlands Bombing Range SD. Analysis of the data showed that the gradient operation attenuated rotor noise by approximately four times and uncompensated maneuver noise by approximately six times as compared to the original total field data. This resulted in overall signal-to-noise roughly five times better than the ORAGS-Arrowhead system. An alternative interpretation of the results is that the Arrowhead detection threshold can be reached at approximately 1.5m higher altitude with the vertical gradient system. The vertical gradient also demonstrated a footprint signature that was 1/2 to 2/3 the size of the total field. This creates the opportunity to successfully detect objects within a more cluttered environment. The improved signal-noise and tighter footprint combined to produce a probability of detection that was 20% higher than the total field system with half the false alarm rate.

We recommend building a production system (which will not require interleaved flight lines) that would have a 12m swath with 1.7m horizontal sensor spacing and 0.5m vertical sensor spacing for most survey altitudes. An adaptation of this system for operation at low altitudes (1.0-1.5m) should also be built. This would have a 6m swath and closely spaced sensors for projects where conditions require very low flying and required the detection of very small targets. Since electronics and peripherals currently exist to support a full production system, only new booms, FAA approval, and additional magnetometers are required.

# 1 Introduction

## 1.1 Background

A series of successful airborne total field magnetic systems have been developed by Oak Ridge National Laboratory (ORNL) and the U.S. Army Engineering Support Center, Huntsville (USAESCH) for the Department of Defense (DoD) Environmental Security Technology Certification Program (ESTCP). An outgrowth of that development is the design and testing of a prototype vertical magnetic gradient (VG) system. As with ground systems, the vertical gradient offers several benefits over a single sensor total field deployment.

At least two categories of magnetic noise influence the effectiveness of airborne systems for UXO mapping and detection. These are rotor noise and maneuver noise. Rotor noise is a type of interference, where a lightly magnetized rotor induces an oscillatory overprint on the sensor data. Maneuver noise, also known as compensation error, is caused by the magnetic properties of the helicopter airframe. This noise could be eliminated by a “perfect” compensation correction, but real corrections always fall short of perfection leaving an uncorrected (or residual) compensation error. The different noise sources cannot be easily separated, and their interrelations are underdetermined. Regardless of their sources, the deleterious effects are largely coherent between two closely spaced sensors in a vertical gradient configuration. As such they are amenable to reduction by subtraction, and reduction by design is preferable to reduction by filtering. As the inability to synthetically model the effects makes it difficult to design improved filters for rotor noise and maneuver noise, the development of a vertical gradient system is a reasonable approach to the problem.

This report describes a series of tests and limited demonstrations of a prototype vertical gradient system, designated the Oak Ridge Airborne Geophysical System – Vertical Gradient (ORAGS-VG). These tests included three 2002 field deployments: Pueblo of Laguna, New Mexico (April), Aberdeen Proving Ground, Maryland (July) and Badlands Bombing Range, South Dakota (September). At all of these sites, additional field tests of the total field magnetometer and/or electromagnetic systems were also conducted. The treatment and results of these other system tests are covered in separate reports.

Analysis of the vertical gradient data focused on signal-noise ratio improvements related to the coherent helicopter noise reduction. In order to provide identical background conditions for a comparison between the gradient and total field technologies, all comparisons are made with respect to the total field measured by the lower sensor of the gradient pair. This minimizes the differences in survey height, helicopter noise conditions, line spacing, interleaving, sensor locations etc. Limited ground truth data were available for this system, and ROC curves have been presented where data permits and showed considerable improvement over the total field results at the same site. These are based on a fully automated picking and discrimination routine.

## **1.2 Objectives of the Demonstration**

The objectives of the demonstration were:

- to demonstrate and quantify the benefits of airborne vertical gradient measurements for unexploded ordnance detection
- to recommend design modifications for a production vertical gradient system

## **1.3 Regulatory Drivers**

Unexploded ordnance (UXO) clearance is generally conducted under CERCLA authority. Attempts to establish a “Range Rule” have been abandoned. In spite of the lack of specific regulatory drivers, many DoD sites and installations are pursuing innovative technologies to address a variety of issues associated with ordnance and ordnance-related artifacts (e.g. buried waste sites or ordnance caches) that resulted from weapons testing and/or training activities. These issues include footprint reduction and site characterization – areas of particular focus for the application of technologies in advance of future regulatory drivers and mandates.

## **1.4 Stakeholder / Enduser Issues**

The Badlands Bombing Range (BBR) and Pueblo of Laguna sites are formerly used defense sites (FUDS). Aberdeen Proving Ground (APG) is an active range. As such, it is important that concentrations of ordnance and locations of possibly live ordnance are mapped so that removal or safeguard actions can be taken where there is the possibility that live ordnance is still in place. It is also important that a permanent record be maintained to document all measurements that are made to support clearance activities. Advanced technology is expected to contribute to the performance of these activities in terms of efficiency as well as cost.

## 2 Technology Description

### 2.1 Technology Development and Application

The ORAGS-VG is based on the sensors, electronics and mounting platform of the total field system (ORAGS-Arrowhead, Figure 2-1a). The primary detection sensor technology uses the same Scintrex CS2 cesium vapor magnetometers and recording console as the total field system. A three-component fluxgate magnetometer is used to compensate for the changing magnetic signature of the aircraft. A dual-phase GPS sensor is used with real-time satellite differential corrections for navigation purposes, and with post-processed base station differential corrections for more accurate data positioning. A laser altimeter is mounted under the center of the aircraft and a four-sensor GPS-based orientation system provides pitch, roll and azimuth data.

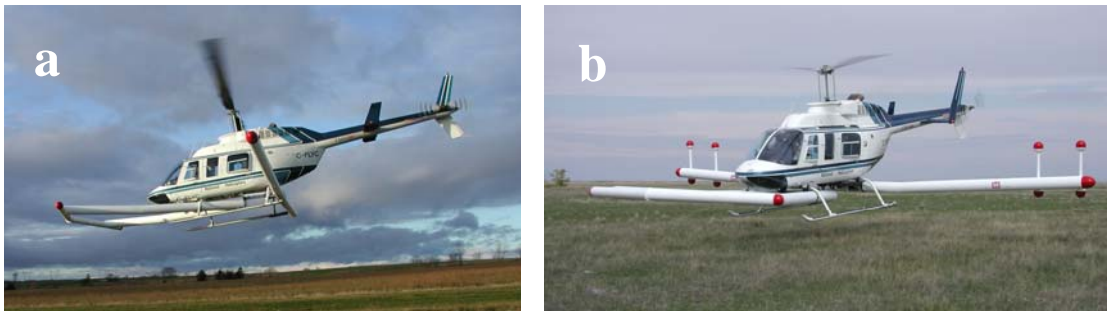


Figure 2-1: Photos of (a) ORAGS-Arrowhead total field magnetometer system and (b) ORAGS-VG vertical magnetic gradient system with 1m vertical and 1m horizontal sensor offsets.

For vertical gradient measurements, magnetometer sensors are mounted in pairs within pods which are attached to the lateral booms (Figure 2-1b). These pods can be configured to place the sensors at 1m or 0.5m vertical offsets, and at 4m, 5m, 5.5m and 6m from the centerline of the aircraft.

### 2.2 Previous Testing of the Technology

ORNL has previously tested several generations of boom-mounted total field airborne magnetometer systems for UXO detection and mapping. The first system was the three sensor HM-3 developed by Aerodat, Ltd., under the direction of J.S. Holladay and T.J. Gamey, and tested by ORNL at Edwards Air Force Base (1997). Subsequent generations included the eight sensor ORAGS-Hammerhead (2000), and the improved ORAGS-Arrowhead (2001). Vertical gradient systems have been flown from fixed-wing and helicopter-towed platforms for a variety of applications (primarily resource exploration), but no boom-mounted vertical gradient system has ever been tested before.

### **2.3 Factor Affecting Cost and Performance**

The cost of an airborne survey depends on several factors, including:

- Helicopter service costs, which depend on the cost of ferrying the aircraft to the site and fuel costs, among other factors.
- The total size of the blocks to be surveyed
- The length of flight lines
- The extent of topographic irregularities or vegetation that can influence flight variations and performance
- The strategic objectives of the survey, specifically high density coverage for individual ordnance detection versus transects for target/impact area delineation and footprint reduction
- The specific ordnance objectives which dictate survey altitude
- The temperature and season, which control the number of hours that can be flown each day
- The location of the site, which can influence the cost of logistics
- The number of sensors and their spacing; systems with too few sensors may require more flying, particularly if they require interleaving of flight lines

The prototype system tested here requires a significant amount of interleaving (minimum three passes to fill a single 12 m swath). Interleaving generally requires a considerable number of reflights in order to obtain consistent coverage over an entire area. This has a direct impact on the cost of the survey. The quality of interleaved lines is also less than optimal because overlapping and crossing flight lines with slightly varying heights cause gridding artifacts that may be mis-interpreted as targets anomalies. This degrades the performance of the system, as well as adding cost for data processing to reduce the detrimental impact.

### **2.4 Advantages and Limitations of the Technology**

This system is subject to the same cost and logistical parameters as the total field technologies. The primary advantage of the vertical gradient system over the total field system is that it is less susceptible to helicopter noise. This is a result of the inherent reduction of coherent or common-mode noise created by the helicopter. The magnetic signature of the helicopter is nearly identical at both sensors in a vertical gradient pair. The placement of the sensor pair horizontally from the helicopter but vertically over the target serves to emphasize the target signature while de-emphasizing the helicopter signature. This enables the processing to use less filtering than would otherwise be necessary for a total field system. Another advantage of the technology is that the vertical gradient signature of a UXO is narrower than its total field signature. This makes it easier to delineate targets in a cluttered environment.

The major limitation of the technology is that the narrower signature requires correspondingly tighter sensor spacing at very low survey altitudes (1-2m). Without tighter spacing, there is a possibility that targets will “fall between the lines” of a survey creating false negative responses.

### 3 Demonstration Design

#### 3.1 Performance Objectives

All quantitative objectives are based on comparison of the vertical gradient response relative to the total field data from the lower sensor of the gradient pair. In particular, the reduction of rotor and maneuver noise are examined. No ground excavation was originally planned for the prototype gradient data collected here, but coincident projects for the total field system provided ground truth at APG. As a result, probability of detection, false alarm rates and ROC curves were calculated at one of the APG sites.

Table 3-1: Performance objectives of vertical gradient system.

Type of Performance Objective	Primary Performance Criteria	Expected Performance (Metric)	Actual Performance Objective Met?
Qualitative	Aerodynamic stability	Safety, certification, no restrictions	Yes Yes Yes
Quantitative	Signal-noise (compared to TF)	Reduction of rotor noise Reduction of FOM	Yes Yes
Qualitative & Quantitative	Detection capabilities	Better delineation of clustered targets, Improved Pd and FA	Yes Yes
Quantitative	Factors affecting technology	Ability to detect targets at 1.5m higher altitude	Yes

#### 3.2 Selecting Test Sites

The airborne survey sites were chosen to enable, where possible, direct comparison of results with the latest airborne total field system, and with ground data where possible. This had the added benefit of minimizing mobilization costs, since both the total field and vertical gradient systems could be deployed on the same field project. The Badlands Bombing Range (BBR) site was nearly ideal in terms of geologic background and topography. Seeded targets were designed to bracket the detection capabilities of the system. The Laguna site was more realistic in that it has slightly rougher terrain, low vegetation and mixed targets with debris. The Aberdeen Proving Ground (APG) was more difficult, featuring high background interference, irregular terrain and more restricted access caused by vegetation. Targets at APG were designed to bracket the detection capabilities.

### 3.3 Test Site History / Characteristics

The BBR demonstration sites consisted of a calibration grid and a partially remediated bombing target. The calibration grid measured 105m x 150m with 52 seeded items. These test items include several types of inert ordnance as well as a number of pipes and other hardware items (Table 4-7). It was intended that the test site include some items that would be too small to be detected by some or all of our systems. Some positions in the grid were unoccupied because they were previously used for surface test objects that were subsequently removed. Their depth of burial, orientation, and length are found in ORNL 2004, and other references. The masses of the objects range from less than 1 kg to more than 50 kg, and depth of burial ranges between 0 and 1.3m.

The second site at BBR was designated Bombing Target 1. This site has been used for several ground and airborne demonstrations and has been partially remediated. The target is divided almost evenly into northern and southern halves by a barbed wire fence. The land on the south side is under cultivation while the land on the north side is range land for livestock. The majority of the ordnance at this location are M38 sand-filled practice bombs.



Figure 3-1: Aerial photo of BBR Bombing Target 1.

The Laguna site included a small calibration grid of surface items, a partially remediated mixed-used bombing target designated Kirtland PBR N-10 and a small site near Kirtland PBR S-12 known as the “Grenade Site”. The calibration grid consisted of several M38 practice bombs on the surface, plus clusters of ordnance debris. During cleanup of the test site it was discovered that one of the debris clusters had been disturbed by livestock. This accounts for a discrepancy between the post-seed ground survey and the airborne survey. The N-10 site has been the subject of previous ground and airborne surveys and has been partially excavated as a result. The majority of the ordnance at this site were M38 practice bombs, although other large ordnance have been found. The “Grenade Site” had not been previously surveyed. Ground observations indicated collections of small debris, but no large ordnance. No ground follow-up was conducted.



Figure 3-2: Photo of central debris mound at Laguna N-10 bombing target.

The Aberdeen Proving Ground site included a calibration grid, a blind seeded grid in clean ground (APG Airfield), and a blind seeded grid in cluttered ground (Mine, Grenade, Direct-fire Weapon Range). The calibration grid included a wide range of ordnance sizes from 60mm to 155mm. This utility of this grid was hampered by a large magnetic anomaly which masked several seeded items in the total field. The vertical gradient was able to resolve these targets more easily.



Figure 3-3: Airphoto showing calibration grid (checkout) and Airfield (open field) sites at Aberdeen Proving Ground.

### 3.4 Present Operations

The BBR and Laguna sites are formerly used defense sites (FUDS). They have been subject to previous geophysical surveys and partial excavation, primarily under the guidance of the ESTCP Program Office. The APG site is an active facility. The calibration grid and the Airfield site (APG Airfield) were located immediately off the runway and were presumably cleared of ordnance during construction. The Mine, Grenade and Direct-fire Weapon Range (APG MGD) was a mixed-use site which has been reported to have been cleared of all ordnance.

### 3.5 Pre-demonstration Testing and Analysis

Tests were conducted to determine the minimum offset distance between sensors before they experienced some form of cross-talk interference. Table 3-2 illustrates that sensors may be placed as close as 20cm without increased noise.

Table 3-2: Sensor noise measured as standard deviation of the signal for different horizontal sensor spacing. Vertical spacing less than 20cm is not possible due to the physical dimensions of the sensors.

Offset (cm)	6	20	40	60	80	100	120	140	160	180
Std dev (pT)	195.4	34.1	32.4	31.8	33.6	32.4	32.1	32.1	32.2	32.2

Shakedown testing of the assembled airborne system and associated components was conducted in Toronto, Ontario, Canada during December 10-21, 2001. The system was test flown by an aeronautical engineer and determined to be completely flight-worthy. Federal Aviation Administration installation certification was subsequently issued.

### 3.6 Testing and Evaluation Plan

#### 3.6.1 Demonstration Set-up and Start-up

Mobilization involved packing and transporting all system components by trailer to the appropriate site and installing them on a Bell 206L Long Ranger helicopter. Calibration and compensation flights were conducted and results evaluated. The eight cesium magnetometers, GPS systems (positioning and attitude), fluxgate magnetometers, data recording console, and laser altimeter were tested to ensure proper operation and performance. The Mission Plan was read and signed by all project participants to assure safe operation of all systems.

#### 3.6.2 Period of Operations

Table 3-3: Period of operations for vertical gradient system tests.

Site	mob	VG ops	(# days)	demob
Laguna	04/10/02	05/01/02-05/02/02	2	05/05/02
APG	07/19/02	07/27/02-07/28/02	2	07/29/02
BBR	09/09/02	10/05/02-10/07/02	3	10/08/02

#### 3.6.3 Area Characterized

Table 3-4: Size of areas characterized in hectares.

Site	Size (ha)
Laguna N-10	9.7
Laguna cal grid	0.7
Laguna Grenade Site	0.5
APG cal grid	1.0
APG Airfield	4.6
APG MGD Range	1.0
BBR cal grid	2.6
BBR BT-1	10.7

#### 3.6.4 Residuals Handling

This section does not apply to this report.

### **3.6.5 Operating Parameters for the Technology**

The ORAGS-VG system is designed for daylight operations only. Parallel lines were flown across the area in a direction dependent upon local logistics and weather conditions. Line spacing varied according to the lateral sensor spacing to achieve a uniform line density. This required interleaving flight lines on all occasions. The eight magnetometers recorded binary data on the console at a rate of 1200 samples per second. A typical survey speed for the system was 100 km/hr. Survey height was 1-3 m above ground level unless specifically required to be higher.

Labor requirements included a geophysical project manager, data processor, pilot, mechanic and system operator. Operations were monitored in real time by the system operator from the in-flight display. Data Quality Control (QC) functions were performed post-flight by the data processor or project manager. QC checks covered GPS quality, diurnal activity, area coverage, magnetic data quality and supplemental data quality (laser altimeter, fluxgate, orientation). Reflights were assigned on a daily basis. Quality Assurance (QA) functions included verification of calibration grid data using ground survey techniques.

### **3.6.6 Experimental Design**

#### *Experimental Variables*

Variable parameters in this system included two vertical sensor separations (0.5m, 1.0m) and three horizontal separations (0.5m, 1.0m, 2.0m). In addition, flight heights were varied over the various calibration grids in order to determine maximum detection offsets for individual targets. To minimize the differences in background conditions, the vertical gradient data are compared to the total field data from the lower sensor of the gradient pair. This provides an excellent basis for measuring relative improvement of the gradient technique over the conventional total field approach because the positioning, processing, filtering, survey height and background noise are identical.

#### *Data processing procedures*

The 1200 Hz raw data were desampled in the signal processing stage to a 60 Hz (Laguna) or 120 Hz (APG/BBR) recording rate. Data were converted to an ASCII format and imported into a Geosoft format database for processing. With the exception of the differential GPS post-processing, all data processing was conducted using the Geosoft software suite and proprietary ORNL algorithms and filters. The quality control, positioning, and magnetic data processing procedures (steps a-i) are described below.

#### *Quality Control*

All data were examined in the field to ensure sufficient data quality for final processing. The adequacy of the compensation data, heading corrections, time lags, orientation calibration, overall performance and noise levels, and data format compatibility were all confirmed during data processing. During survey operations, flight lines were plotted to verify full coverage of the area. Missing lines or gaps in acquisition were reacquired. Data were also examined for high noise levels, data drop outs, significant diurnal activity, or other unacceptable conditions. Lines flown, but deemed to be unacceptable for quality reasons, were re-flown.

### *Positioning*

During flight, the pilot was guided by an on-board navigation system that used real-time satellite-based DGPS positions. This provided sufficient accuracy for data collection (approx 1m), but was inadequate for final data positioning. To increase the accuracy of the final data positioning, a base station GPS was established at pre-existing U.S. Geodetic Survey monuments.

Table 3-5: Locations of GPS base station monuments.

Laguna	Albuquerque International Airport Secondary Control Point	NAD83 35° 02' 11.51050" N 106° 37' 17.19129" W 1605.50m
APG	Martin Municipal Airport Primary Control Point	NAD83 39° 19' 57.88957" N 076° 25' 38.50226" W 6.311m
BBR	Cuny Table	NAD83 43° 31' 13.5870" N 102° 41' 53.8915" W 1085.3m

Raw data in the aircraft and on the ground were collected and post-processed to apply differential corrections. The final latitude and longitude data were projected onto an orthogonal grid using the North American Datum 1983 (NAD 83) UTM projection in meters. Vertical positioning was monitored by laser altimeter with an accuracy of 2cm. No filtering was required of this data, although occasional drop-outs were removed.

### *Magnetic data processing procedure*

The magnetic data were subjected to several stages of geophysical processing. These stages included correction for time lags, removal of sensor dropouts, compensation for dynamic helicopter effects, removal of diurnal variation, correction for sensor heading error, array balancing, and removal of helicopter rotor noise. The analytic signal was calculated from the corrected residual magnetic total field data.

#### (a) Time Lag Correction

There is a lag between the time the sensor makes a measurement and the time it is time stamped and recorded. This applies to both the magnetometer and the GPS. Accurate positioning requires a correction for this lag. Time lags between the magnetometers, fluxgate magnetometer, and GPS signals were measured by a proprietary ORAGS firmware utility. This utility sends a single pulse that is visible in the data streams of all three instruments. This lag was corrected in all data streams before processing.

#### (b) Sensor Dropouts

Cesium vapor magnetometers have a preferred orientation to the Earth's magnetic field. As a result of the motion of the aircraft, the sensor dead zones can occasionally align with the Earth's field. In this event, the readings drop out, usually from an average of 50,000 nT to 0 nT. This usually only occurs during turn-around between lines, and rarely during actual data acquisition. All dropouts were removed manually before processing.

#### (c) Aircraft Compensation

The presence of the helicopter in close proximity to the magnetic sensors results in considerable deviation in the readings, and generally requires some form of compensation. The orientation of the aircraft with respect to the sensors and the motion of the aircraft through the earth's magnetic field are also contributing factors. A special calibration flight is performed to record the information necessary to remove these effects. The maneuver consists of a square or rectangular-shaped flight path at high altitude to gain information in each of the cardinal directions. During this procedure, the pitch, roll and yaw of the aircraft were varied. This provided a complete picture of the effects of the aircraft at all headings in all orientations. The entire maneuver was conducted twice for comparison. The information was used to calculate coefficients for a 18-term polynomial for each sensor. The fluxgate data were used as the baseline reference channel for orientation. The polynomial is applied post flight to the raw data, and the results are generally referred to as the compensated data.

The compensation was applied using two different methods. The first was to derive coefficients to correct the total field data before calculating the vertical gradient, while the second was to calculate the vertical gradient and then derive coefficients for the vertical gradient. Both techniques produced the same results. For consistency in comparing total field to vertical gradient data, the former technique was used throughout.

#### (d) Magnetic Diurnal Variations

The earth's magnetic field changes constantly over the course of the day, sometimes drastically. This means that measurements made in the air include a randomly drifting background level. A base station sensor was established near the GPS base station to monitor and record this variation every five seconds. The time stamps on the airborne and ground units were synchronized to GPS time. The diurnal activity recorded at the base station was extremely quiet. In general, diurnal variations were less than 5nT per survey line. Processing included defaulting repeated values and linearly interpolating between the remaining points. Data were monitored for extreme activity which would necessitate reflights of collected data.

#### (e) Heading Corrections

Cesium vapor magnetometers are susceptible to heading errors. The result is that one sensor will give different readings when rotated about a stationary point. This error is usually less than 0.2 nT. Heading corrections were applied to adjust readings for this effect as part of the regional removal process.

(f) Array Balancing

These magnetic sensors also provide a lower degree of absolute accuracy than relative accuracy. Different sensors in identical situations will measure the same relative change of 1 nT, but they may differ in their actual measured value, such as whether the change was from 50,000 to 50,001 nT or from 50,100 to 50,101 nT. After individual sensors are heading-corrected to a uniform background reading, the background level of each sensor is corrected or balanced to match one another across the entire airborne array. This correction is also encompassed in the regional removal.

(g) Regional Removal

Deep-seated, large scale background geology and some cultural features which contribute to the local regional magnetic field were removed using a combination of filtering and splining techniques. The output is a residual magnetic total field. This process also removed all diurnal, heading and balancing effects.

(h) Rotor Noise

The aircraft rotor spins at a constant rate of approximately 400 rpm. This introduces noise to the magnetic readings at a frequency of approximately 6.6 Hz. Harmonics at multiples of this base are also observable, but are much smaller. This frequency is usually higher than the spatial frequency created by near surface metallic objects. This effect has been removed with a low-pass frequency filter.

(i) Analytic Signal

The data resulting from this survey are presented in the form of analytic signal. The square root of the sum of the squares of the three orthogonal magnetic gradients is the total gradient or analytic signal. It represents the maximum rate of change of the magnetic field with change in position.

For the total field systems, this parameter is calculated from the gridded residual total field data using simple directional differences for the horizontal gradients and FFT routines for the vertical gradient (first derivative of total field). The vertical gradient system uses FFT routines to calculate the total field (first integral of the vertical gradient) and then calculates horizontal gradients from this.

There are several advantages to using the analytic signal. For small objects, it is somewhat more straightforward to interpret visually than total field or vertical gradient data. Both total field and vertical gradient measurements typically display a dipolar response signature to small, compact sources, having both a positive and negative deviation from the background. The actual source location is a point between the two peaks, as determined by the magnetic latitude of the site and the properties of the source itself. Analytic signal is more symmetric about the target, is always a positive value and has less dependence on magnetic latitude. Analytic signal maps present anomalies as low intensity to high intensity shapes.

The prototype configuration of the ORAGS-VG also allows the direct measurement of horizontal gradients. This provides the opportunity to calculate the analytic signal directly without FFT algorithms. There are both advantages and disadvantages to this system. In addition to suppressing some helicopter noise (1.5x improvement in signal-noise ratio), it avoids the tendency of FFT routines to emphasize data positioning errors as they appear in the total field. Horizontal gradients do, however, risk missing targets by bracketing them between sensors so that they subtract out close to zero.

### **3.6.7 Sampling Plan**

This section does not apply to this report.

### **3.6.8 Demobilization**

De-installation was carried out by dismounting the booms from the helicopter frame and the re-packing the sensors and instruments in shipping containers. The containers were placed in a trailer for transport to ORNL.

## 4 Performance Assessment

### 4.1 Performance Criteria

The most significant performance criterion was the signal-noise ratio. This provided a direct comparison to the total field system, whose performance is well documented in the relevant ESTCP reports. Since this is a prototype system with a wide variety of operating characteristics (sensor spacing, etc), performance metrics such as productivity and demonstrated probability of detection have not been calculated directly, except by reference to the Arrowhead system.

The demonstrated effectiveness is determined by comparison to the total field data over the same targets. No dedicated excavation of vertical gradient targets was planned or executed, although some areas were coincident with ground follow-up for the total field system. Without ground follow-up, calculation of probability of detection and generation of ROC curves was not possible. Instead, performance changes are measured relative to the established total field approach.

Only at the Aberdeen Proving Ground test grid was it practical to construct an estimated ROC curve. It should be noted that the ROC curve of the calibration grid is optimized based on the full knowledge of the ground truth, and the curve for the blind test is based on a limited number of excavation points and not a full validation. Both curves, however, represent a fully automated approach to both detection and discrimination.

Table 4-1: Performance Criteria

<b>Performance Criteria</b>	<b>Description</b>	<b>Importance</b>
Aerodynamic stability (safety)	Does not hamper safe operation of the aircraft.	Primary
Aerodynamic stability (certification)	Passes FAA certification requirements.	Primary
Aerodynamic stability (no restrictions)	Does not require additional ballast or any other additional flight restrictions.	Primary
Signal-noise (rotor noise)	Shows an improvement in the signal-noise ratio through lower rotor noise than the equivalent total field data. This will improve detection of smaller objects by reduction of high frequency noise.	Primary
Signal-noise (compensation)	Shows a relative improvement in the Figure of Merit (FOM) over the equivalent total field data. The FOM is a measure of the reduction of the airframe maneuver noise and will improve detection of smaller objects by reduction of low frequency noise.	Primary
Detection capabilities	Can detect targets amid higher levels of background clutter. Anomalies should be more sharply defined with a narrower footprint. Pd and FA where possible.	Primary
Factors affecting technology	Has fewer operational limitations than the Arrowhead system in terms of topography and vegetation. In particular, it should demonstrate the ability to detect items from higher altitudes.	Primary

## 4.2 Performance Confirmation Methods

Direct comparison of the ORAGS-VG vertical gradient data to the ORAGS-Arrowhead total field results has many constraints. For example, the actual survey height will not be the same for both systems at any given point. This will have the effect of differentially improving anomalous responses. Also, the current vertical gradient system requires interleaved flight lines and will have different line density than the Arrowhead system. All of these factors serve to alter the “signal” in the signal-noise ratio comparisons. The alternative is to compare the ORAGS-VG vertical gradient data to the ORAGS-VG total field data of the lower sensor. This solves the problems associated with line density, height fluctuations, positional errors and interleaving and provides a common basis for evaluation of the helicopter and rotor noise effects.

There is also a problem in comparing systems with different units of measure – in this case nT and nT/m. The signal-noise ratio solves this problem in most cases, but there are also occasions where no convenient “signal” is present or desirable. This is the case at high altitudes where aeromagnetic maneuver noise is being measured. For this we rely on measurements of a theoretical signal acquired in survey mode. Conveniently, for a dipole response at heights between 1.5 and 7.0m, total field in nT and vertical gradient in nT/m are numerically equivalent within a factor of two. That is, at 3.2m, a theoretical dipole producing a 1nT total field peak also produces a 1nT/m vertical gradient peak. This is demonstrated graphically with synthetic data in Figure 4-12 and with real data in Figure 4-6 and Table 4-3. In the calculation of the signal-noise for compensation corrections, we therefore use a theoretical signal of 1nT for the total field and 1nT/m for the vertical gradient.

Having established a method for comparable “signal” measurements, standardized “noise” measurements must be determined. For high frequency rotor noise, the standard deviation of the total field or vertical gradient data over a representative section of flat background readings will be used. For low frequency compensation noise, the Figure of Merit (FOM) and Improvement Ratio (IR) will be used. The FOM is a measure of the residual aircraft signature after compensation. It consists of the sum of the peak-peak noise in each of the twelve separate parts of the compensation maneuver.

$$FOM = \sum noise_{ij}$$

where noise = average residual peak-peak deflection,  
and I = cardinal direction (N, S, E, W)  
and j = maneuver (pitch, roll, yaw).

The Improvement Ratio is the ratio of the standard deviation of the raw/residual peak-peak deflections.

Table 4-2: Expected performance and performance confirmation method

<b>Performance Criteria</b>	<b>Expected Performance Metric (Pre-demo)</b>	<b>Performance Confirmation Method</b>	<b>Actual Performance (Post-demo)</b>
Aerodynamic stability (safety)	Same flight characteristics as Arrowhead	Successful test flight, favorable report from pilot and aeronautics engineer	Same flight characteristics as Arrowhead
Aerodynamic stability (certification)	FAA approval	STC award	FAA approval and STC awarded
Aerodynamic stability (no restrictions)	No ballast required	STC specifications	No ballast requirements on STC
Signal-noise (rotor noise)	Rotor noise reduced by 5x	Measured rotor noise	Rotor noise reduced by 4x
Signal-noise (compensation)	FOM improved by 5x	Measured FOM	FOM reduced by 6x, IR no change
Detection capabilities	Better delineation of clustered targets	Visual inspection of data, spectral analysis	Confirmed, VG footprint is 1.5-2x narrower
Detection capabilities	Improved Pd and FA	Comparison to total field results at APG	Pd increased by 20%, FA reduced by half
Factors affecting technology	Ability to detect targets at 1.5m higher altitude	Comparison of test grid data from multiple heights	Targets detectable at 1.5m higher altitude

## 4.3 Data Analysis, Interpretation and Evaluation

### 4.3.1 Aerodynamic Stability

Test flights of the prototype design were conducted at National Helicopters home base in Bolton, Ontario in December, 2001. The pilot reported that the addition of the vertical gradient pods did nothing to change the qualitative flight characteristics of the Arrowhead system. The aeronautics engineer recorded data for weight and balance, and airborne performance through a variety of maneuvers such as autorotation. These and subsequent tests resulted in the award of FAA approval, Supplemental Type Certificate (STC) SH03-32, which has no requirement for ballast.

### 4.3.2 Rotor Noise

The most prominent noise in helicopter magnetic data is related to the rotor head assembly and blades. A time series of total field rotor noise for a typical airborne profile is shown in Figure 4-1. Mapping the high frequency components of the total field helicopter noise demonstrates a generally symmetric and roughly circular distribution around the body of the helicopter with a logarithmic falloff with lateral distance from the center (Figure 4-2). The logarithmic decay coefficient was calculated at  $-0.29$  (Figure 4-3), which means that the noise drops by roughly half with every meter of distance from the helicopter.

Figure 4-4 compares vertical gradient time series data at three locations along the boom (4, 5 and 6m from the center) and demonstrates the noise fall-off shown in Figure 4-2. As the sensors are moved closer to the helicopter, the gradient noise at 6.5 and 13Hz becomes more characteristic of the total field rotor noise shown in Figure 4-1. The total field does not exhibit this change in character with position along the boom. For the total field, only the amplitude decreases, not the character of the waveform. This indicates that the rotor noise correlation (i.e. relative amplitude and phase between upper and lower sensors) is not constant along the boom. This is consistent with the view that the dominant source of noise is the rotor mast head assembly, which is above the sensors and centered on the aircraft. Had the dominant source been some other part, or parts, that were lower on the airframe (and therefore at the same relative distance from the two sensors), the noise correlation would presumably have been stronger and more uniform along the length of the boom. Similarly, if the blades had been the dominant source, the correlation would have been weaker but more uniform along the length of the boom.

The major rotor noise source therefore is the yoke at the head of the rotor mast, which has a small permanent magnetization and rotates at approximately 400 rpm (for the B206L helicopter). This has been confirmed by Gauss-meter readings of the mast and blade assembly, and is the result of imperfect de-Gaussing after mandatory FAA non-destructive testing of the component. Extreme cases can result in noise on the order of tens of nT. The rotor blades have much smaller magnetic signatures and appear at a frequency double that of the main rotor mast for a two bladed helicopter. In time series, these harmonics may be seen as smaller deflections against the background of the rotor mast signal (Figure 4-1), depending on their phase alignment with the larger signal. The

blade effect is independent of the rotor-head magnetization, and is not visible against the background of a poorly de-Gaussed rotor head. It is therefore believed to be the result of a separate phenomenon, probably eddy currents flowing in the blades. As such, they are dependent on the speed and direction of the aircraft and rotor segment with respect to the sensor and the Earth's magnetic field at any given time.

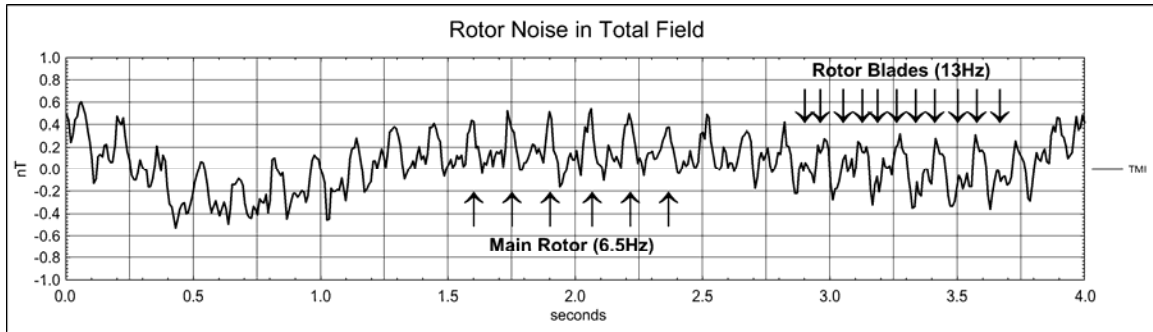


Figure 4-1: Time series of total field magnetic response illustrating helicopter rotor noise.

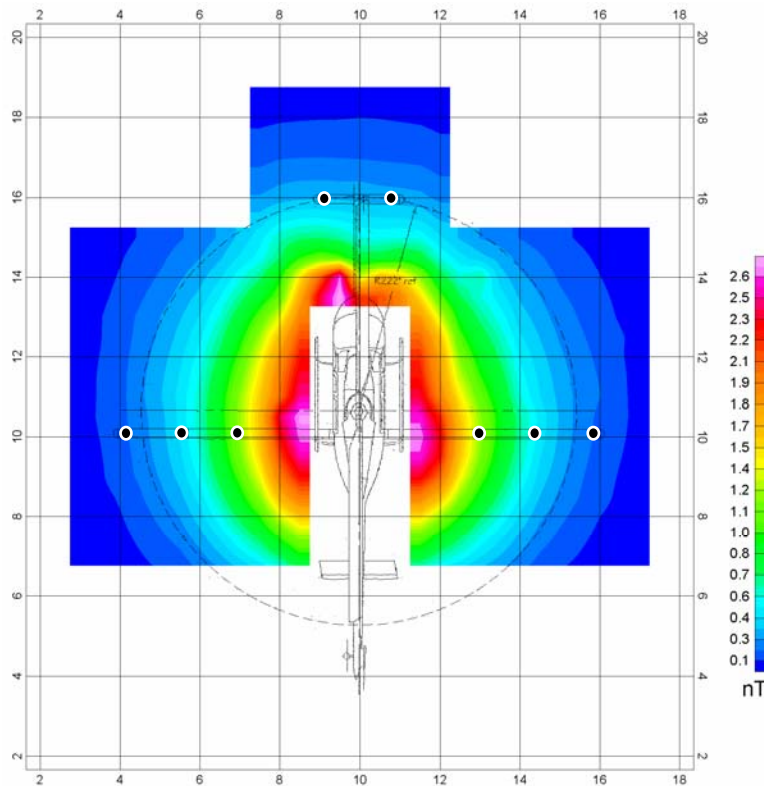


Figure 4-2: High frequency total field magnetic noise distribution about a helicopter. Dots show location of sensors from ORAGS-Hammerhead configuration. Lateral sensor locations correspond to 2.6m, 4.3m and 6.0m from helicopter centerline.

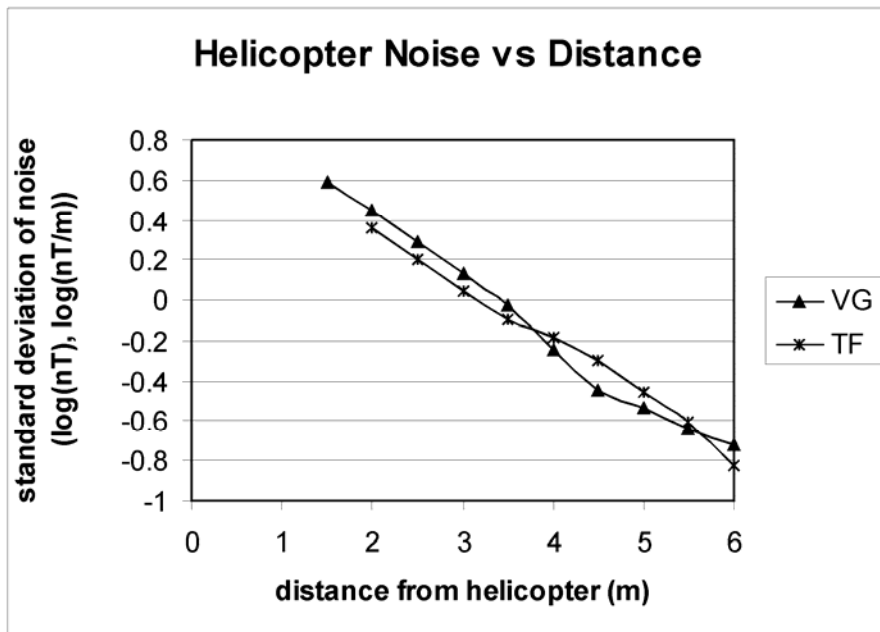


Figure 4-3: High frequency total field and vertical gradient noise vs distance from centerline of helicopter.

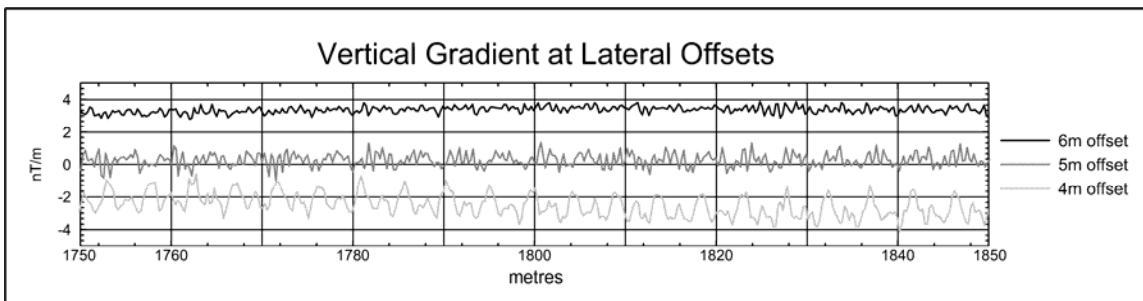


Figure 4-4: High frequency vertical gradient measurements at various locations along the lateral boom.

A spectral analysis of the raw total field and vertical gradient data (Figure 4-5) show sharp peaks at 6.48Hz and 12.9Hz corresponding to the main rotor and rotor blades respectively. Smaller and broader peaks at 2.15Hz and 3.30Hz are vibration harmonics of the main rotor peak. The source of the peak at 11.8Hz is unexplained, but appears consistently in all data sets, and may be vibration-induced. The broader peak that appears at 5.8Hz may be a vibration harmonic of this, but does not appear in all data sets. The small broad peak at 15Hz is also unexplained. The low frequency peak in the total field at 0.76Hz is the result of maneuver noise as discussed in the next section.

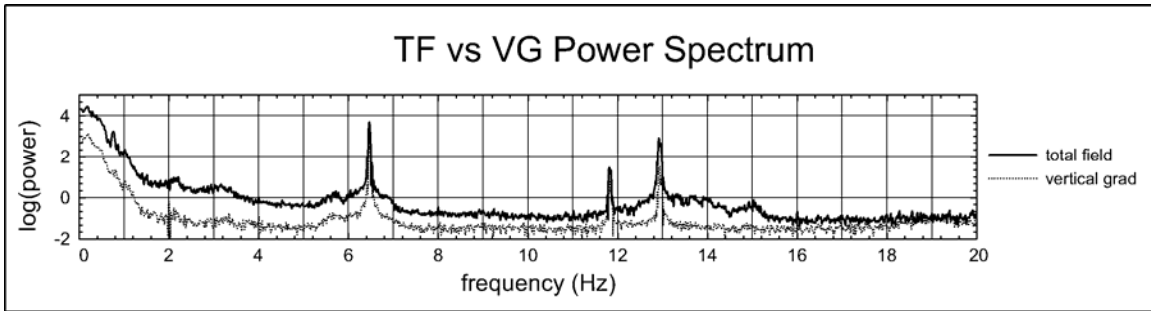


Figure 4-5: Power spectrum of total field and vertical gradient data while airborne.

An example of raw profile data over a series of small UXO targets is shown in Figure 4-6. Using the standard deviation of measurements during the helicopter turn immediately preceding the survey line as a measure of rotor noise, signal-noise ratios are calculated for the total field and vertical gradient as shown in Table 4-3. As described in section 4.2, the standard deviation of the data over a representative section of flat background readings is used as a measure of rotor noise in the signal-noise calculations. The signal is the peak-peak measure of the individual anomalies. Identical filters were applied to total field and gradient data. The vertical gradient shows an estimated improvement in signal-noise of four times over the total field response. The vertical gradient profiles in Figure 4-6 are from the sensors positioned 5m from the center of the helicopter using a 1.0m vertical separation. Sensors at the tip of the boom show lower amplitude noise levels and consequently higher signal-noise ratios, but the improvement from total field to vertical gradient remains the same at approximately four times.

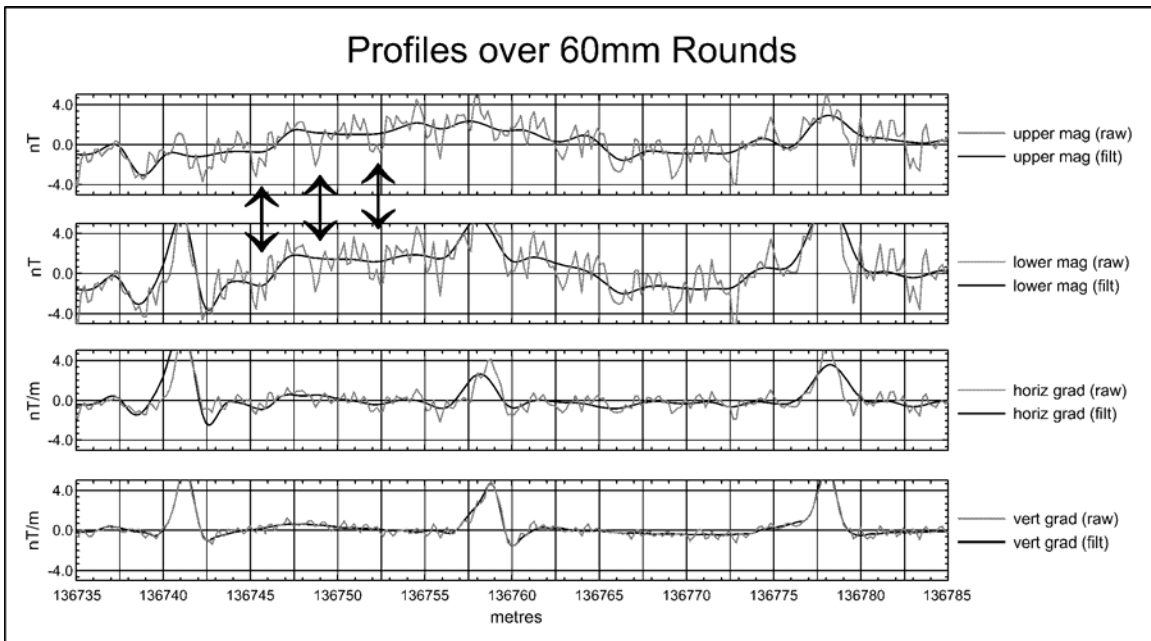


Figure 4-6: Profiles over three small UXO targets. Note coherent total field noise between upper and lower sensors at arrows, and subsequent attenuation in vertical gradient. Targets are 60mm illumination rounds, average height of lower sensor is 0.9m. Peak values reported in Table 4-3.

Table 4-3: Calculation of signal-noise ratios for total field (TF), vertical gradient (VG), horizontal transverse gradient (HG) and horizontal longitudinal gradient (LG), based on the three anomalies shown in Figure 4-6.

Anom	TF (nT)	filtered S/N	VG (nT/m)	filtered S/N	S/N improve
s-dev noise		0.4nT		0.09nT/m	
1	9.4	23.5	7.1	78.9	3.4
2	6.5	16.3	6.1	67.8	4.2
3	7.2	18.0	7.2	80.0	4.4
ave	7.7	19.3	6.8	75.6	3.9
Anom	TF (nT)	filtered S/N	HG (nT/m)	filtered S/N	S/N improve
s-dev noise		0.4nT		0.2nT/m	
1	9.4	23.5	9.6	48.0	2.0
2	6.5	16.3	3.3	16.5	1.0
3	7.2	18.0	3.8	19.0	1.1
ave	7.7	19.3	5.6	27.8	1.4
Anom	TF (nT)	filtered S/N	LG (nT/m)	filtered S/N	S/N improve
s-dev noise		0.4nT		0.2nT/m	
1	9.4	23.5	7.1	35.5	1.5
2	6.5	16.3	3.8	19.0	1.2
3	7.2	18.0	7.2	36.0	2.0
ave	7.7	19.3	6.0	30.2	1.6

### 4.3.3 Maneuver Noise

The second of the two dominant helicopter noise sources is maneuver noise. This is the result of the incomplete removal of effects associated with the presence of a magnetic or conductive airframe moving through the Earth's magnetic field. Compensation for this effect is accomplished by subtraction of an 18-term polynomial (Hardwick, 1986). The first three terms account for the permanent magnetization of the aircraft. The next six terms account for the magnetic field induced in the airframe. The final nine terms account for eddy currents created within the airframe. The magnetic effects of the airframe are independent of the effects of the rotor in terms of their amplitude, spectral content and vertical gradient correlation at the sensor locations.

Polynomial coefficients are determined by correlation of the total field response to the direction cosines of the helicopter orientation as measured by a three-component fluxgate magnetometer. Data to calculate these coefficient terms are collected in a special "compensation flight". This consists of flying a square flight pattern at high altitude, and distinctly varying the aircraft pitch, roll and yaw in each of the four directions to produce twelve different maneuver responses. Improvements in the system noise are computed as a Figure of Merit (FOM) or as an Improvement Ratio (IR). The IR may be thought of as a measure of relative effectiveness, while the FOM is an absolute measure of effectiveness. The FOM is calculated as the sum of the remaining peak-peak noise after correction in each of the twelve parts of the compensation flight. The IR is calculated as the average ratio of the standard deviations of the noise before and after correction. Perfect compensation would produce a FOM equal to 12x the system noise floor, and an IR equal to the uncorrected noise divided by the noise floor. For fixed wing operations, a typical compensation will produce a FOM of 1nT and an IR of 5. Boom-mounted helicopter operations typically produce a total field FOM of 10nT and an IR of 15. Calculations based on these numbers will show that raw helicopter maneuver effects (i.e. FOM before compensation correction<sup>1</sup>) for boom-mounted systems is approximately 30 times those of fixed wing operations.

Figure 4-7 illustrates one section of a compensation maneuver (south-bound, yaw) using a 1m vertical sensor separation. The raw maneuver effect is 16.3nT in the total field and 2.5nT/m in the vertical gradient. As these are different units of measure, calculations of signal-noise ratios use a theoretical signal of 1nT for the total field and 1nT/m for the vertical gradient as demonstrated above. Accepting this justification for comparison purposes, the signal-noise ratio in the uncompensated data is reduced by a factor of 6.5 times for the gradient system as compared to the total field system as a result of correlation between the two sensors. After compensation, the remaining peak-peak deflections are 1.1nT and 0.19nT/m, implying a signal-noise benefit of 5.8 times for the gradient system.

---

<sup>1</sup> FOM(before) = FOM(after) x IR

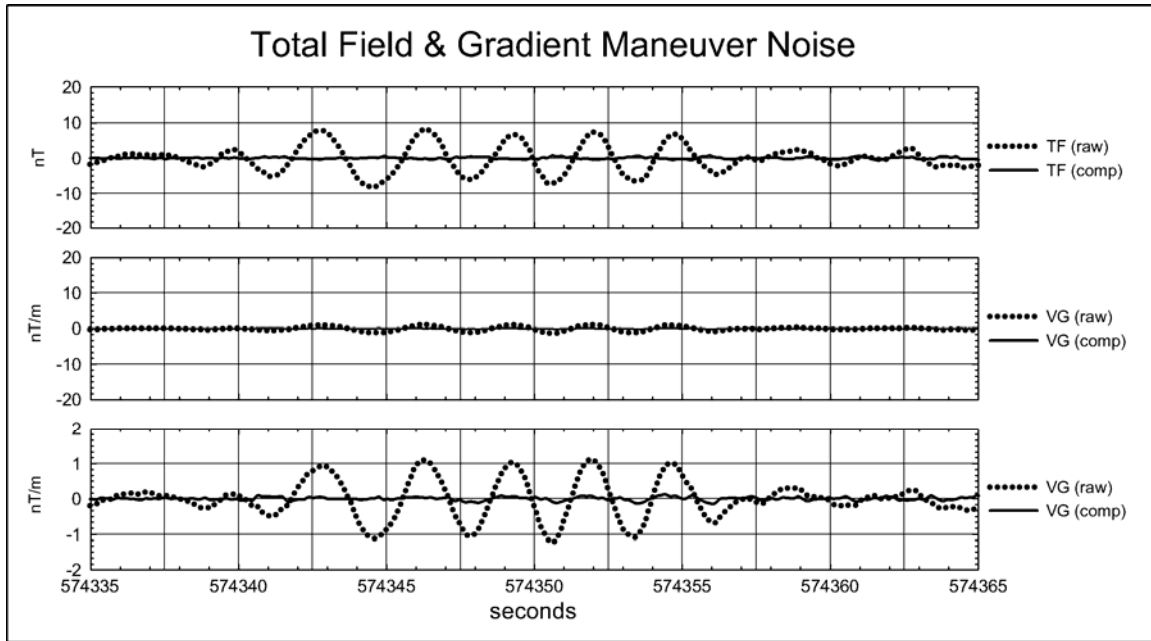


Figure 4-7: Sample of total field and vertical gradient maneuver noise. Comparison of the top two panels (raw TF to raw VG) illustrates the improved FOM of the vertical gradient. Comparison of the top and bottom panels (raw to comp for both TF and VG) illustrates the consistency of the IR.

These numbers also provide an Improvement Ratio of 15 for the total field system and 13 for the vertical gradient system. This implies that the correlation between the helicopter orientation and the deviations observed at the sensors is the same for the total field as it is for the vertical gradient. This is verified by a second test. Compensation of vertical gradient data can be conducted either by compensation of each total field sensor followed by calculation of the gradient (comp/grad), or by calculation of the gradient and then compensation (grad/comp). A comparison of the two approaches produced negligible differences (on the order of rounding error), implying that the compensation routine produced an equal improvement in the total field as the vertical gradient. In order to maintain a consistent basis for comparison between total field and vertical gradient, data presented here have compensation applied before calculation of the gradient.

Even before the compensation is applied, the calculation of the vertical gradient demonstrates a significant reduction in maneuver noise, as seen in Figure 4-7. Total peak-peak noise is reduced in all twelve parts of the compensation flight. Although the IR numbers are similar for both the total field and vertical gradient, the FOM for the vertical gradient has improved by approximately six times.

Although the effects of maneuver noise in actual survey data are difficult to isolate from those of other noise sources, the suppression of maneuver noise can be seen in 2D data plots. Long, linear trends approximately 15m long, following flight lines (corresponding to 0.75Hz at 20m/s) are indicative of residual maneuver noise. Generally, any single sensor noise of sufficiently low frequency that cannot be otherwise accounted for is assumed to be maneuver noise (after elimination of overlapping lines that cause gridding

and interpolation artifacts), although it may also encompass some low frequency vibration or orientation noise. Vibration noise would presumably be correlated between the gradient sensors also. Orientation noise will appear as location errors which are coincident with maneuver noise, which is also related to aircraft orientation. Gridded data (Figure 4-8, over the same three targets as the profiles in Figure 4-6) show these effects. The first order analytic signals derived from the total field and from the vertical gradient are presented here in order to provide a common base for a direct comparison of the two techniques. For the total field, the analytic signal is calculated as the square-root of the sum of the squares of the directional gradients. In the case of the vertical gradient, the horizontal gradients are calculated from the FFT integral of the measured gradient. Both rotor noise and maneuver noise are considerably reduced in the vertical gradient as a result of its natural cancellation of correlated noise.

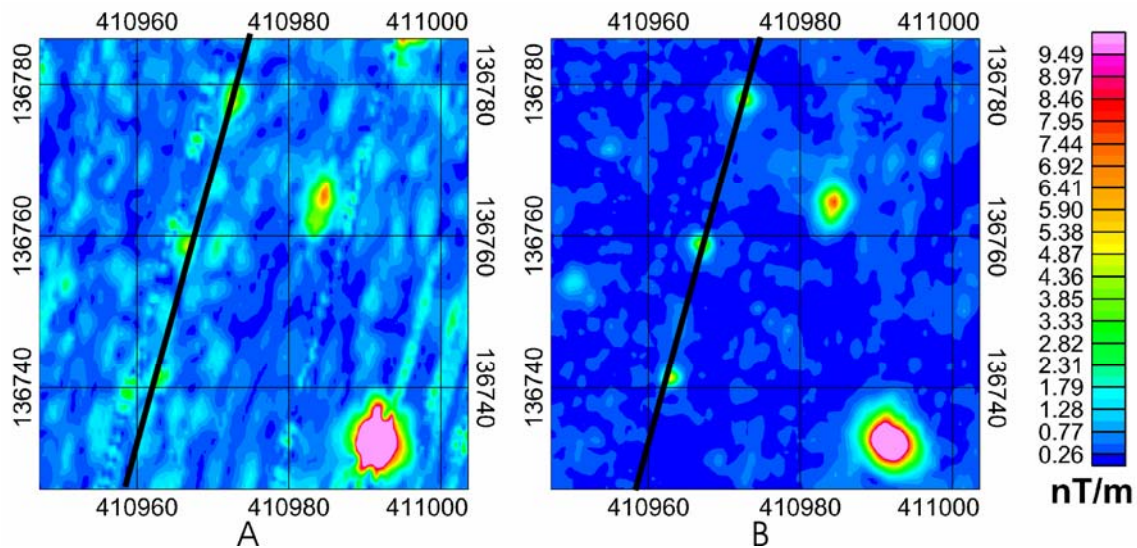


Figure 4-8: First order analytic signal derived from (a) total field (lower sensor) and from (b) vertical gradient data over a calibration grid. Horizontal units in meters, average height of lower sensor 0.9m. Black line represents path of profile from Figure 4-6. Line-line deflections in the total field-based results demonstrate uncompensated maneuver noise accentuated by grid splining.

#### 4.3.4 Altitude and Positioning Errors

As mentioned above, low frequency noise may also be introduced by factors other than the magnetic expression of the aircraft during maneuvering. Errors in the position and altitude of individual sensors may be introduced in many ways. These factors are common to total field and vertical gradient techniques, but have different effects on each. A brief review of their implications is presented.

Assuming flat and level flight, GPS positioning errors, which may be as large as 0.2m after post-processing, will be constant across a data swath (8 data lines acquired during one pass of the aircraft), but can be problematic when combining data from multiple passes. This is particularly true where the data were acquired in two opposite flight directions with opposite cross-winds and obstacles. When aircraft orientation data are inaccurate, the magnitude and sign of positioning errors will vary with distance from the GPS antenna location. For this prototype ORAGS-VG with sensors on the lateral booms only and the GPS antenna in the center of the forward boom, this effect is at its worst. For example, with 5° of uncorrected yaw, position errors increase by approximately 0.8m.

To date, vertical gradient data have not been acquired with gradiometers in the foreboom. In its current configuration, the ORAGS-VG system, described previously, requires interleaved flight lines in order to achieve full coverage at 1.7m line separation. Interleaving creates its own set of problems. The separations between individual sensor lines are more variable, and prone to gaps and overlaps in map view.

Altitude uncertainties cause significant perturbations in calculated vertical gradient maps. When magnetometers are operated at altitudes of 30m AGL, a +/-0.5m range in altitude is reasonable to maintain. This causes an increase or decrease in the anomaly strength of +/- 4.6% in total field, or +/-5.1% in vertical gradient. At a mean altitude of 1.5m, which is typical for an airborne UXO survey, we typically encounter variations in altitude of +/-0.25m or more. These are not exclusively a function of the precision with which the pilot can maintain a specific altitude at 60 knots air speed, but are also associated with perturbations in the topography of the survey area. The helicopter must maintain a safe distance above the highest local point in the flight swath, and this differs from one swath to the next. The difficulty of maintaining a constant draped altitude contributes an additional complication. For total field measurements, the +/-0.25m variation in altitude can result in a variation in the magnetic field of about +/-35%. With vertical gradient, this results in an error of about +/-40 %.

Compensation is used to correct magnetic data for changes in the magnetic effect of the aircraft associated with its orientation and position relative to each magnetometer. Beyond the aircraft's magnetic field, perturbations in roll and pitch, similarly, contribute uncertainties in the sensor altitude from the assumed altitudes. It is common for pitch and roll to vary within a range of +/-3°. The pitch (front-to-back rotation) has its greatest effect on the foreboom sensors, and the roll has its greatest effect on the sideboom sensors. A +/-3° pitch can cause +/-0.34m change in the altitude of the foreboom sensors, and a +/-3° roll can cause +/-0.31m change in altitude of the sideboom magnetometers.

Thus these effects can be larger than the “pilot control” effects discussed in the previous paragraph. The two effects combine linearly, causing potential changes in the altitude of some sensors during some portions of a flight line of about 0.6m.

Errors and noise that are not removed from profile data will be carried into the gridding stage where they will cascade into additional errors. These include gridding errors as well as errors associated with transforms and filters used to generate other map products, e.g. gradients and analytic signal. Processing methods should be chosen that will minimize the extent to which profile errors are enhanced in gridded map products.

The effect of positioning errors on vertical gradient grids will be different from that of equivalent total field grids. The narrower footprint of the gradient leaves less opportunity for poorly positioned lines to distort the shape of gridded anomalies. Positioning errors that would be readily apparent in a total field map often drop below the noise threshold in the vertical gradient. The coordinates of the peak location are no more accurate, but automated routines to find the peaks have less gridding noise to contend with.

### 4.3.5 Delineation of Clustered Targets

A spectral analysis of total field and vertical gradient dipole anomalies shows that vertical gradient anomalies are always narrower than total field anomalies for small UXO targets (Figure 4-9). Comparisons of dipole response spectra show that vertical gradient anomalies have higher frequency content, and their spectral peak is twice the wave-number (or twice the frequency assuming a constant survey speed) of the total field. This would indicate that the strongest part of the vertical gradient signature has half the footprint of the total field signature. As a result, anomalies from closely-spaced objects are less likely to overlap (more distinct peaks) in the vertical gradient. This is the theoretical foundation for the premise that a vertical gradient system will better-distinguish between closely spaced peaks than a total field system.

Although rotor noise has a much narrower spectral peak than magnetic dipole signatures, the spectrum partially overlaps that of near surface anomalies and has a peak amplitude comparable to many small UXO targets. The proximity of the rotor noise peak to that of the modeled anomaly peaks is shown in Figure 4-9, where the survey altitude (offset distance) is assumed to be 2m and the survey speed is 20m/s. When flying lower and faster, this problem is accentuated because ground anomalies are pushed into higher frequencies towards the filter cut-off for the rotor noise. At the maximum safe speed and lowest possible survey height this may cause ringing, but because the gradient is naturally less susceptible to rotor noise, filter requirements can be correspondingly reduced and the overall sensitivity is improved.

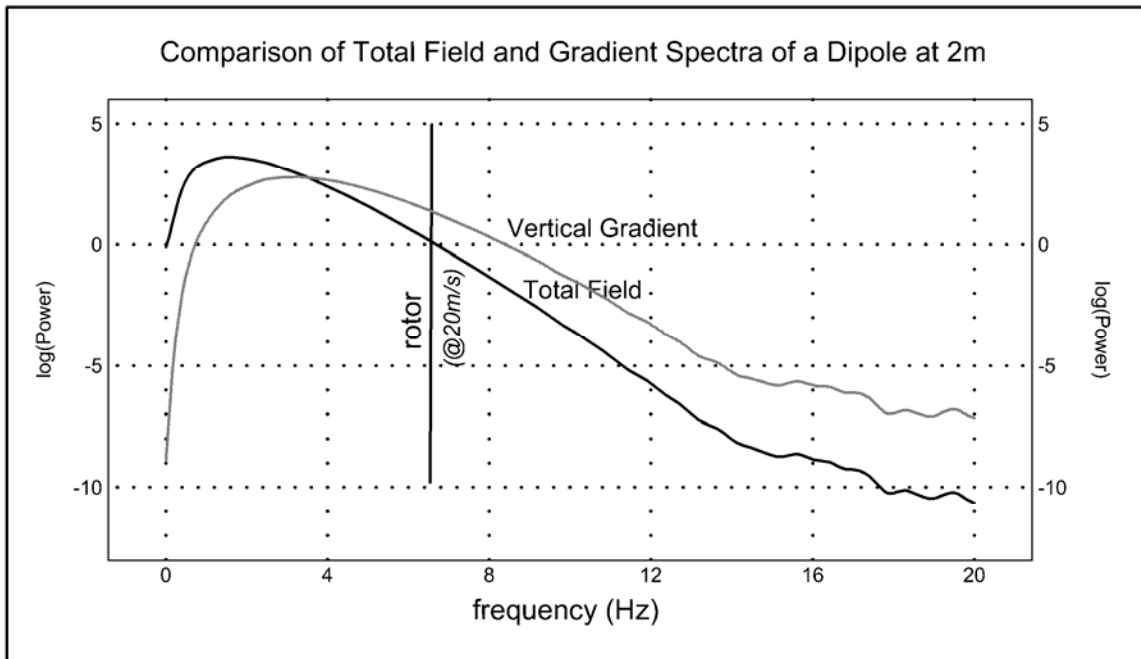


Figure 4-9: Power spectra of the total field and vertical gradient signature of a dipole.

Similarly, profile modeling can be used to demonstrate the narrower footprint of the vertical gradient. Figure 4-10 shows two total field profiles over a modeled horizontal dipole at different heights. The vertical gradient is the difference between the two. Assuming no remanent magnetization (induced only), the calculated anomaly for a N-S horizontal dipole at 1.0m depth and a N-S flight line at 1.5 AGL, has a total field half-width of about 2.6m (Figure 4-10). The half-width of the total field profile at 2.5m AGL is about 3.5m. This corresponds with the common rule-of-thumb that the half-width is equivalent to the source-sensor separation. The half-width of the vertical gradient profile (measured at 3.0m AGL) is about 2.2m. Whereas the total field half-width is equal to the separation distance, the vertical gradient half-width is closer to  $2/3$ . This complements the spectral analysis above which showed the peak vertical gradient frequency to be  $1/2$  the wavelength of the total field.

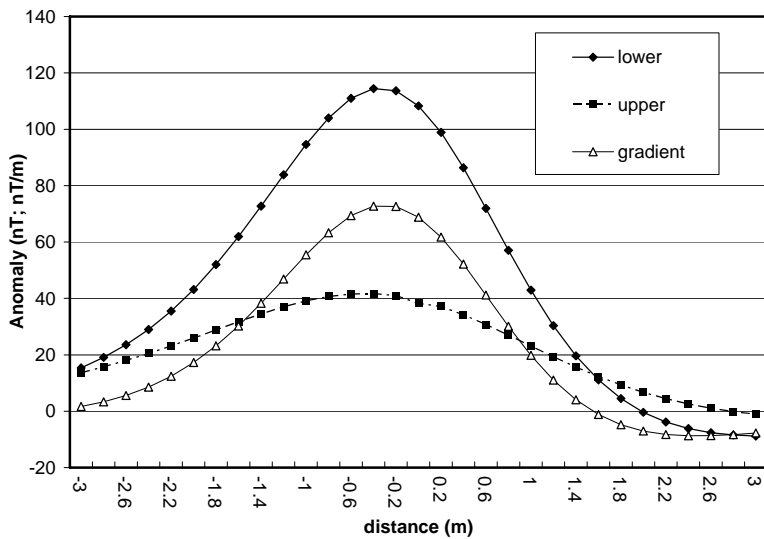


Figure 4-10: Calculated total field for a horizontal dipole at 1m depth with upper and lower magnetometers at 1.5m and 2.5m AGL, and the resulting measured vertical gradient.

Measured data confirms these theoretical findings. An extract from Bombing Target 1 on Cuny Table at BBR (Figure 4-11) shows how tightly clustered anomalies inside the circular target halo are more cleanly defined, as are the anomalies near the fence. The first data set is the analytic signal derived from the lower sensor total field measurements, while the second map is the analytic signal derived from the vertical gradient measurements.

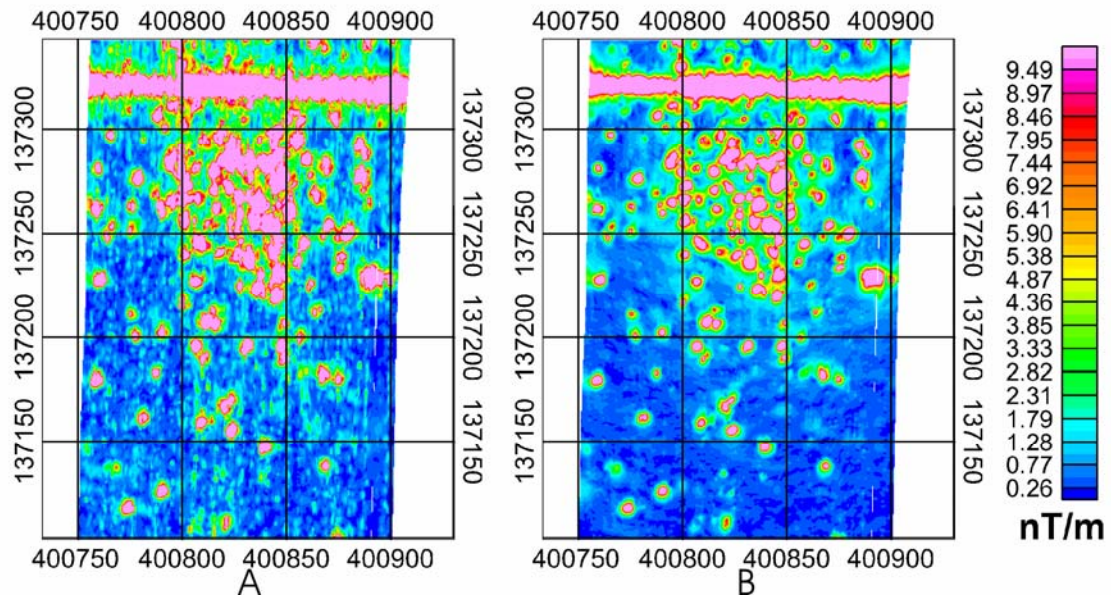


Figure 4-11: Extract of analytic signal over Cuny Table Bombing Target 1. Data are derived from (a) lower sensor total field and (b) measured vertical gradient.

### 4.3.6 Increased Altitude

Based on the five times improvement in signal-noise ratio expected of the vertical gradient system, targets can be detected with the vertical gradient at 1.5m higher survey altitude than with the total field. The actual improvement achieved was 6 times in the maneuver noise and 4 times in the rotor noise. Figure 4-12 demonstrates a five time lower noise threshold (0.5nT to 0.1nT/m, assuming a nominal source-sensor offset between 2-5m) increases the limiting detection height by 1.5m. Models were based on the peak response of a 25A/m dipole in a vertical field and vertical sensor separation of 0.2m.

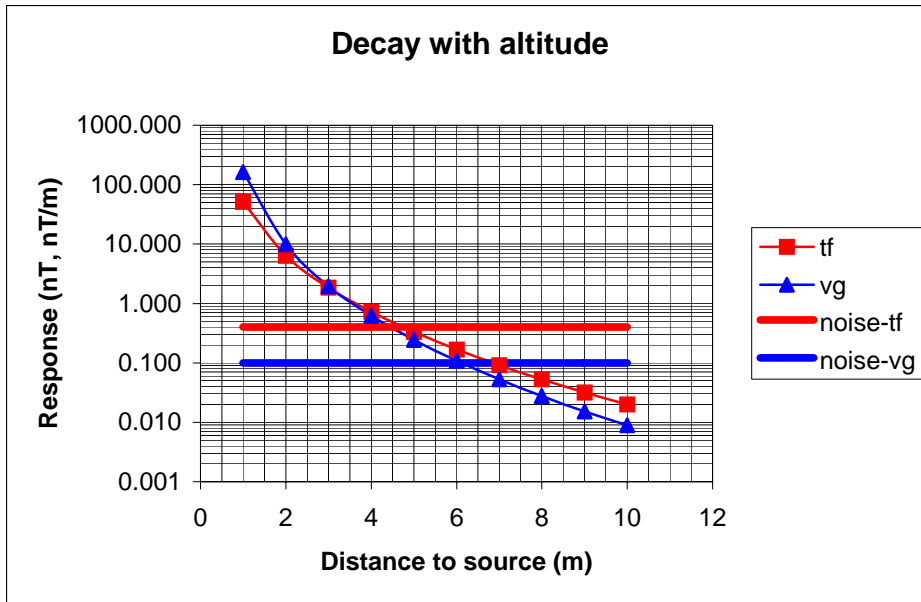


Figure 4-12: Peak response vs depth for a simple dipole. The numeric equivalence of nT and nT/m for a narrow band of low altitudes is demonstrated. Representative noise levels with a 5:1 advantage in signal-noise for the vertical gradient show a 1.5m height advantage.

This was verified at the Laguna calibration site (Figure 4-13) which was flown at four heights in 1.5m increments. The data show that targets which are barely visible in the vertical gradient derived data are missing from the total field derived data (solid vs hollow arrows). These targets are detectable with the same signal-noise ratio in the total field derived data at an altitude 1.5m lower than the vertical gradient derived data (solid vs solid arrows). This confirms the theoretical calculations that a 1.5m altitude advantage is derived from the vertical gradient system.

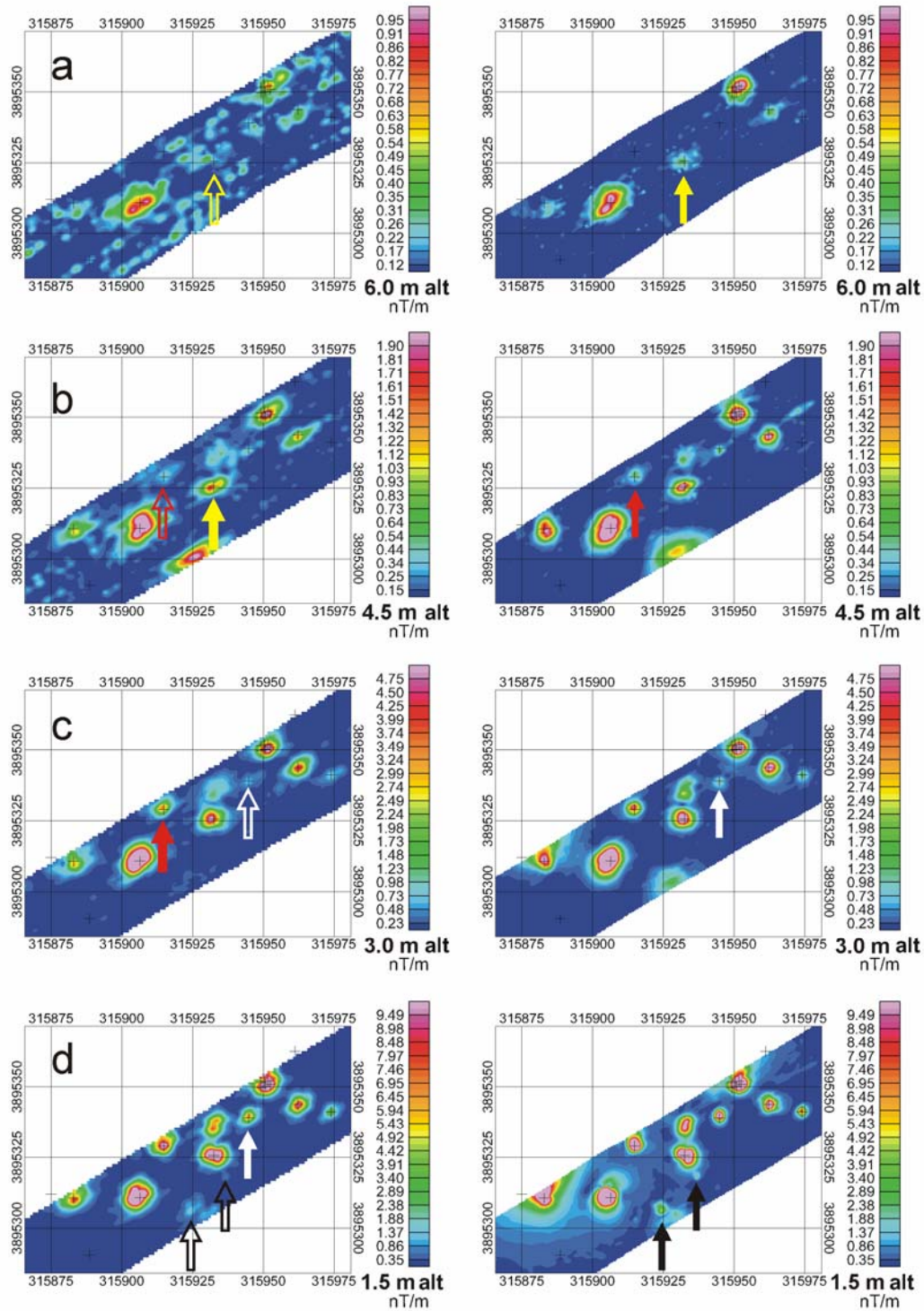


Figure 4-13: Laguna Test Grid analytic signal derived from lower sensor total field (left side) and from vertical gradient (right side) at various heights. Color coded arrows indicate anomalies on the threshold of detection. Solid arrows would be above the threshold, hollow arrows would be below the threshold.

### 4.3.7 Horizontal Gradients

The current configuration of the ORAGS-VG also allows horizontal gradients to be measured, as demonstrated previously in Figure 4-6. In general, this was found to provide a small increase in the signal-noise ratio over the total field, but not as much of an improvement as the vertical gradient (Table 4-3).

In gridded format, the horizontal gradient also appears to be less susceptible to maneuver noise than the total field. Figures 4-14 & 4-15 show a comparison of the total field, transverse horizontal gradient, longitudinal horizontal gradient and vertical gradient over the same area as Figure 4-8. Whereas Figure 4-8 showed the data using a common format (analytic signal), this was not practical with the horizontal gradient, so comparisons must take into account the fact that these are three different parameters with three different units. The seven UXO items in this portion of the test site (as identified in Figure 4-15) are three 60mm mortars, two 81mm mortars, one 2.25-in rocket, and a 1.55mm artillery shell.

The total field is derived from the lower sensors in the gradient pods. Transverse gradients were determined as the difference between measurements in adjacent pods. Simulations of the longitudinal gradient (in-line with the aircraft) were also conducted by taking the time derivative of the lower sensors. The time base was selected to match the rotor frequency in order to minimize the rotor noise (approximately 3.25m). A 1m baseline (approximately 0.05s) was tested for comparison against the 1m transverse and vertical gradients, but this approach only served to enhance the rotor noise as it comprised only 1/3 of a rotor rotation. The disadvantage of the longitudinal gradient is that narrow anomalies are about the same width as the rotor noise, which further reduces the utility of this simulated gradient. Any noise correlation demonstrated by this approach also assumes that the noise is identical from one rotation and the next. Actually measuring the longitudinal gradient would produce better results than this simulation. Such a configuration would display better amplitude correlation than the transverse gradient, but would require a slight correction for phase lag of the rotor position.

The sensors constituting the transverse gradient are at different distances from the helicopter in this lateral boom configuration, which implies that the helicopter noise should be less well correlated. While the phase remains the same, the amplitudes are different. A ground target may also appear as a correlated source in this case. There is a risk that the pair of magnetometers in the horizontal gradient will “bracket” a near surface anomaly and measure a zero or significantly reduced gradient amplitude. This would result in a false negative response in the horizontal gradient that would not occur in either the total field, vertical gradient or longitudinal gradient.

It should also be noted that the measurement altitude for the horizontal gradient is 0.5m lower than the center point of the vertical gradient. The HG grids also display more distortions that can be attributed to uncompensated maneuver noise than the vertical gradient, although less than the total field. This implies that the fall-off of the maneuver effect with distance from the helicopter, as measured by the difference between two sensors at different distances from the helicopter center, is quite small.

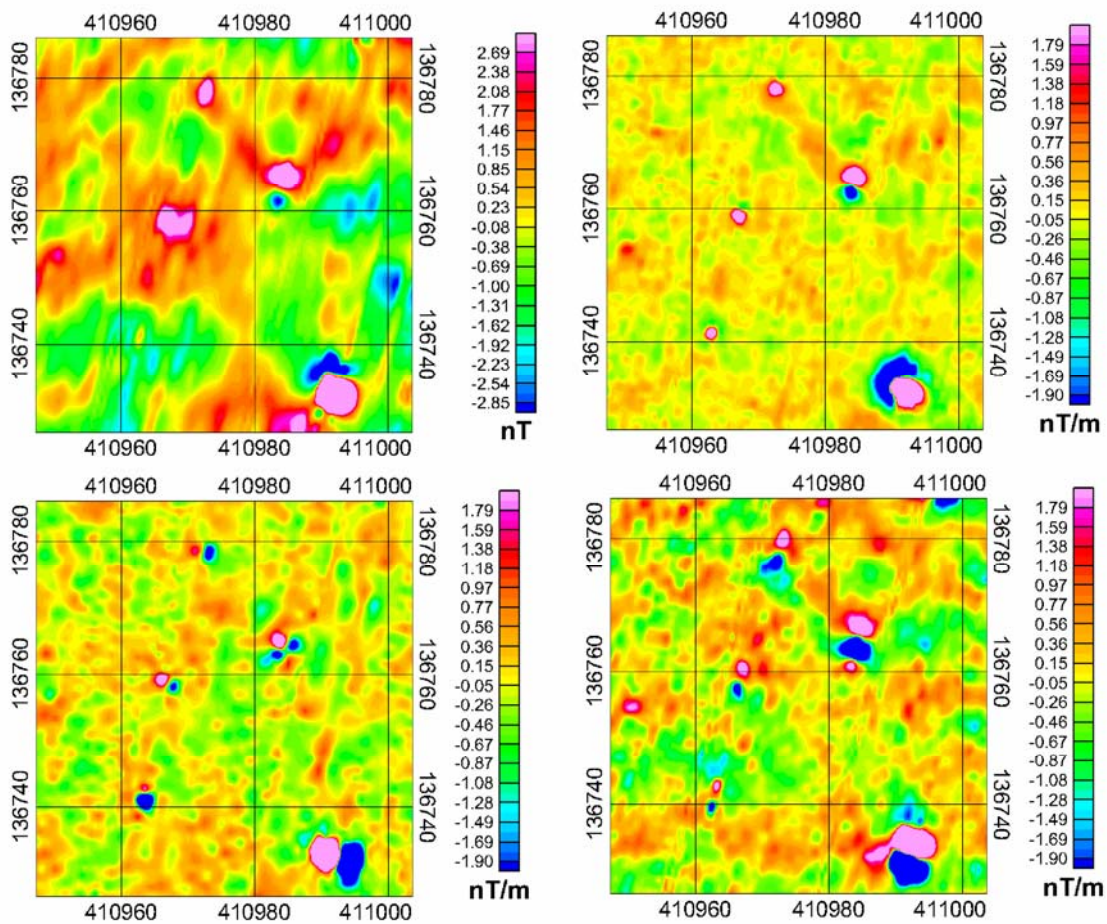


Figure 4-14: Contour maps of total field (top-left), vertical gradient (top-rt), transverse horizontal gradient (bot-left) and longitudinal horizontal gradient (bot-rt). Same data set as Figure 4-8 and the profile from Figure 4-6. Note the reduction of maneuver noise from the original total field, to calculated longitudinal gradient, measured horizontal gradient and measured vertical gradient (highest to lowest noise). Horizontal units in meters.

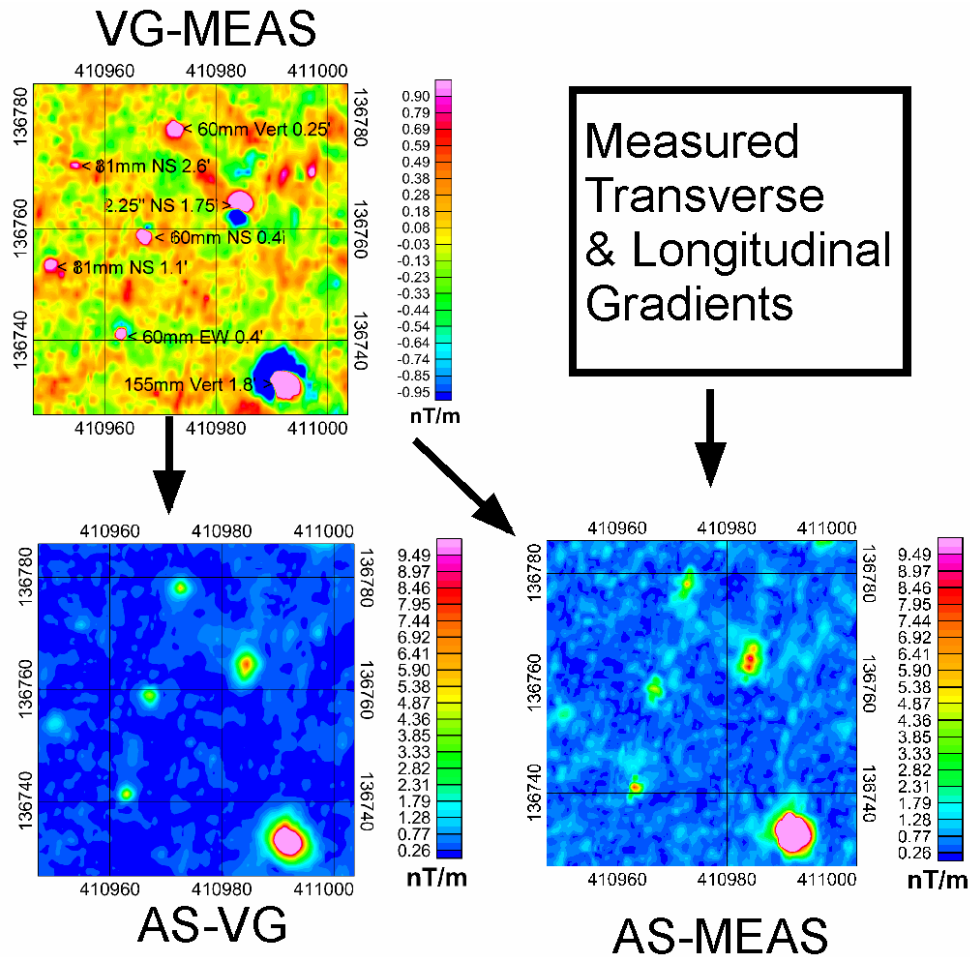


Figure 4-15: Comparison of analytic signal maps derived from calculated vs measured horizontal gradients. Measured vertical gradient (vg-meas) is combined with FFT grid-calculated horizontal gradients to produce one version of the analytic signal (as-vg). It is also combined with the measured horizontal gradients to produce a second version of the analytic signal (as-meas). The noise reduction inherent in the horizontal gradients is better than that in the total field, but not enough to create a better analytic signal map.

We have already compared the analytic signal derived from the total field to that from the vertical gradient for this area in Figure 4-8. Another alternative is to calculate the analytic signal directly from the measure gradients, thereby bypassing any potential distortions cause by FFT routines. Figure 4-15 shows that line parallel noise due to uncorrected rotor or compensation noise, combined with altitude and positioning errors is still a factor in the directly measured analytic signal.

### 4.3.8 Field Results

The following sections examine survey results on a location-by-location basis. There is some overlap with the previous sections because data from these sites were used to study specific problems related to system performance. This section follows the system development chronologically in a case study approach. The emphasis here is on qualitative analysis rather than the quantitative performance metrics discussed earlier.

#### *Field Results – Laguna*

This section examines the field results from the Pueblo of Laguna survey sites in New Mexico, May 2002. This represented the first field deployment of the vertical gradient system after the initial weight and balance certification test flight. It covered three principle areas: a test grid, Bombing Target N-10 and the Grenade Site.

In addition to the area coverage, an initial test of the variation of helicopter noise with distance from the helicopter was conducted. This involved collecting measurements from a vertical gradient pod at positions along the lateral boom. These results are shown in Figure 4-3. This demonstrated that the amplitude fall-off of vertical gradient noise was the same as total field noise.

The first survey grid was the test grid. This was flown at four altitudes and the results are shown in Figure 4-13. This demonstrated the overall improvement in signal-noise ratio and the 1.5m increase in survey height that was possible with the vertical gradient system. A list of target items is provided in Table 4-4.

The test grid and the N-10 bombing target were both flown with a 1m and 0.5m vertical sensor separation. The 0.5m separation demonstrated lower noise levels than the 1m separation (Figure 4-16). It was also observed that the vertical gradient pods vibrated excessively about the axis of the boom. This was determined to be the result of boom distortion due to the torque applied by the longer pod. Boom re-enforcements were introduced to counter this problem in subsequent tests. The results presented in this section for N-10 and the Grenade Range are for the 0.5m vertical separation.

Table 4-4: Laguna Calibration Site seed items including the eight inert ordnance casings (or pieces of ordnance) and two iron stakes.

Easting	Northing	ID	Description	Angle	Weight (lb.)	Length (in.)	Diam (in.)	Notes
315963.16	3895364.56	NE	corner	*	*	*	*	
315975.92	3895343.17	NW	corner	*	*	*	*	
315890.54	3895292.60	SW	corner	*	*	*	*	
315876.97	3895314.07	SE	corner	*	*	*	*	
315884.84	3895312.65	T-1	M-38	150	6.00	32.00	7.50	
315908.33	3895312.81	T-2	M-38 w tail fin	0	7.50	43.00	7.50	
315916.74	3895331.00	T-3	M-38 w tail fin	50	10.00	33.00	7.50	
315934.47	3895327.65	T-4	M-38 w tail fin	100	9.00	35.00	7.50	
315952.72	3895352.22	T-5	M-38 no tail fin	170	3.50	31.00	7.50	M38 badly decomposed
315954.50	3895352.99	T5a	tail fin, fin assembly	*	3.00	17.00	10.00	72" from M38
315953.59	3895353.98	T5b	fin assembly	*	1.00	10.00	5.00	69" from M38
315952.40	3895354.03	T5c	2 tin cans, 7 disks	*	2.00	24.00	24.00	69" from M38, scattered on 24" circle
315951.24	3895353.54	T5d	fin assembly, metal sheet	*	1.00	12.00	12.00	79" from M38, scattered on 12" square
315951.16	3895351.68	T5e	2 fin assemblies	*	1.50	15.00	4.00	72" from M38
315953.64	3895349.83	T5f	tail fin	*	2.00	8.00	8.00	102" from M38, moved by cow
315964.25	3895345.76	T-6	tail, 3nose, flange, 3det	*	14.00	60.00	60.00	scattered over 60" circle, wt is total

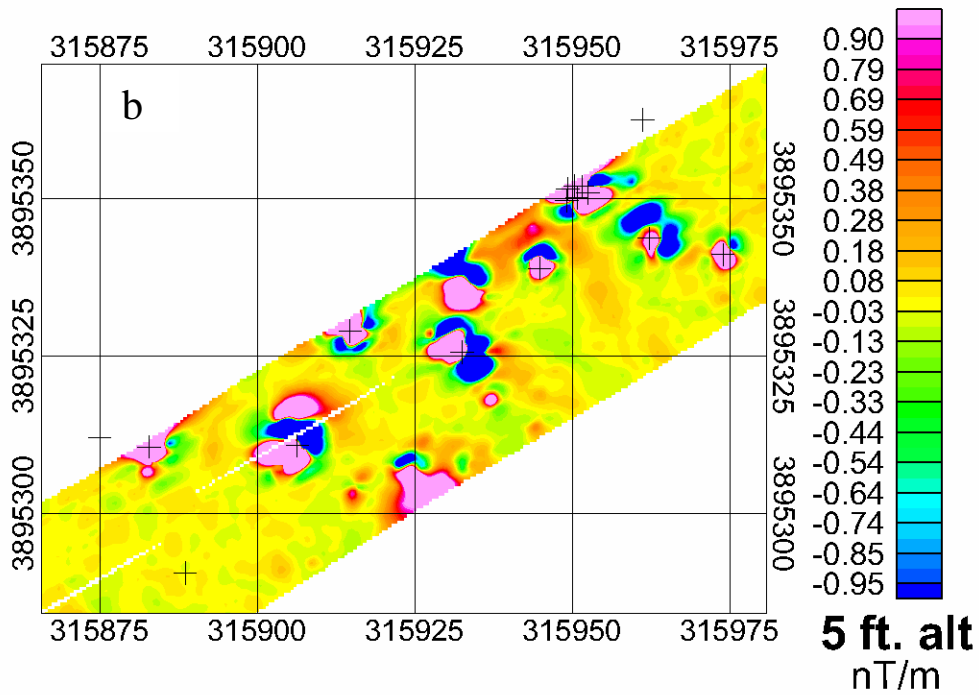
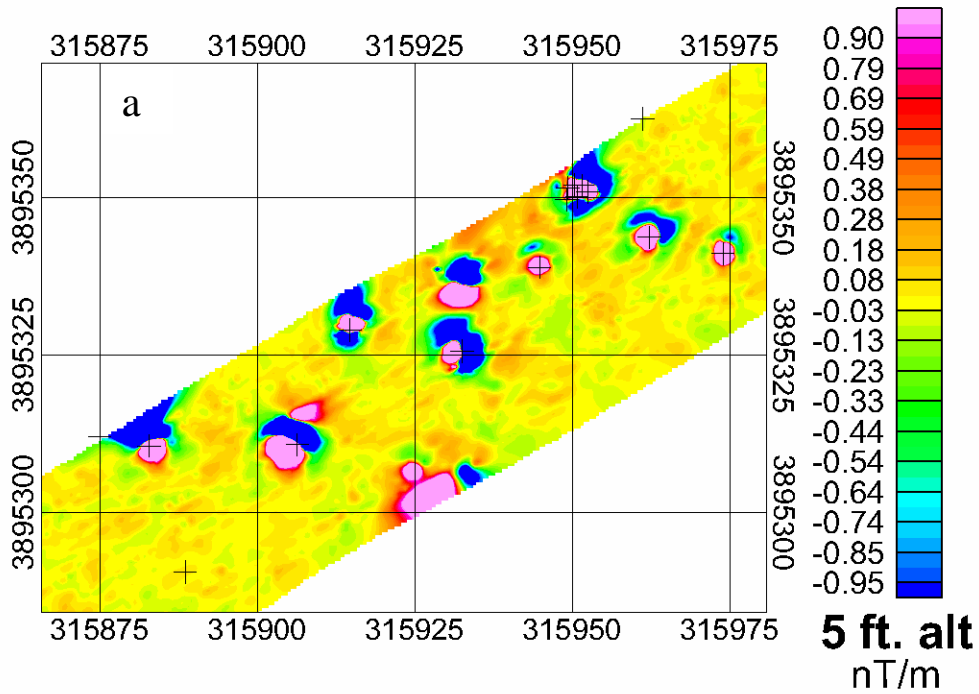


Figure 4-16: Comparison of vertical gradient data at the Laguna test grid for the (a) 1m and (b) 0.5m vertical sensor separations. Horizontal separations were 1m and lines were interleaved. The 1m vertical separation showed slightly higher noise levels due to excessive pod vibration.

Data were acquired in a long strip through the center of Bombing Target N-10. This provided the opportunity to examine a full range of ordnance densities. The full survey section is shown in Figure 4-17, with extracts in Figure 4-18. Target lists were provided from this data set, but ground excavations were selected from the associated total field array results. There was a small area of overlap between the TF excavations and VG survey data (approx 0.17ha), but this was entirely within the high density area of the target where individual targets could not be distinguished. All excavated anomalies were reported as caused by UXO fragments. As a result, they are not discussed here.

The comparison between the total field and vertical gradient results in Figure 4-18 shows how correlated noise has been systematically reduced to improve the overall signal-noise ratio. Individual anomalies are clearly defined and sharply isolated from neighboring effects. Down-line effects (single trace EW trends approximately 15m long) correspond to the 0.75Hz compensation errors and have been effectively eliminated. Background values have been slightly elevated in the analytic signal calculation. This is due to the influence of the strong central response of the bombing target on the FFT integral calculation required in the analytic signal calculation from vertical gradient. In spite of this, smaller anomalies are still better defined in the vertical gradient data than the total field.

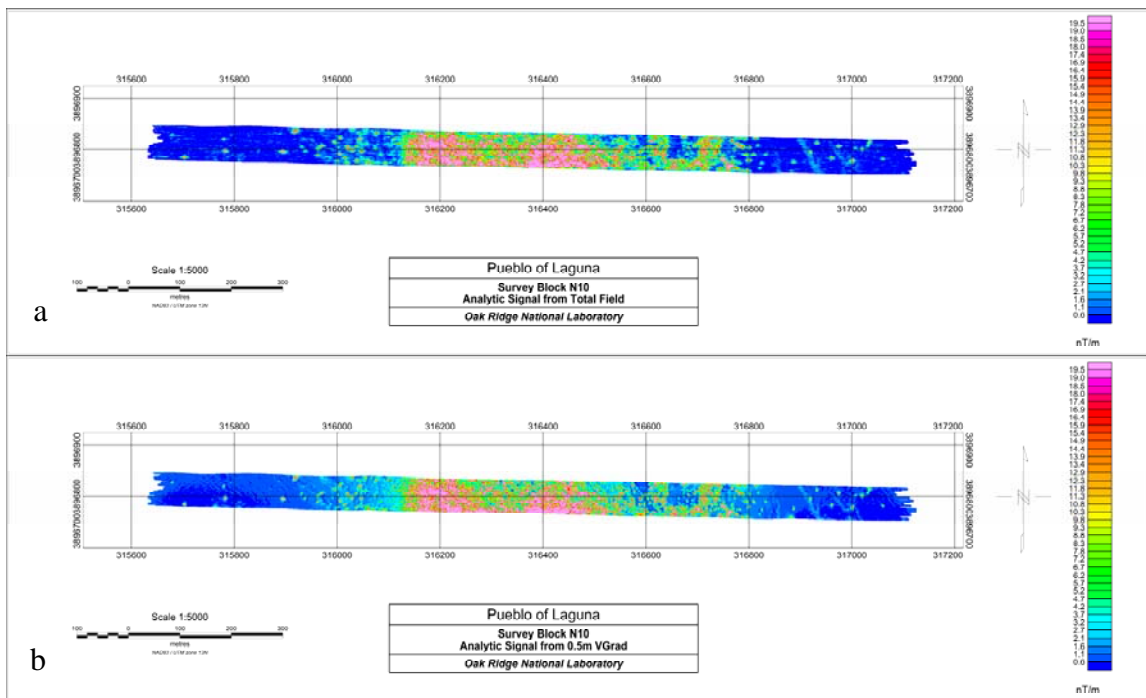


Figure 4-17: Analytic signal map over N-10 bombing target derived from (a) the lower sensor total field data and (b) the vertical gradient data.

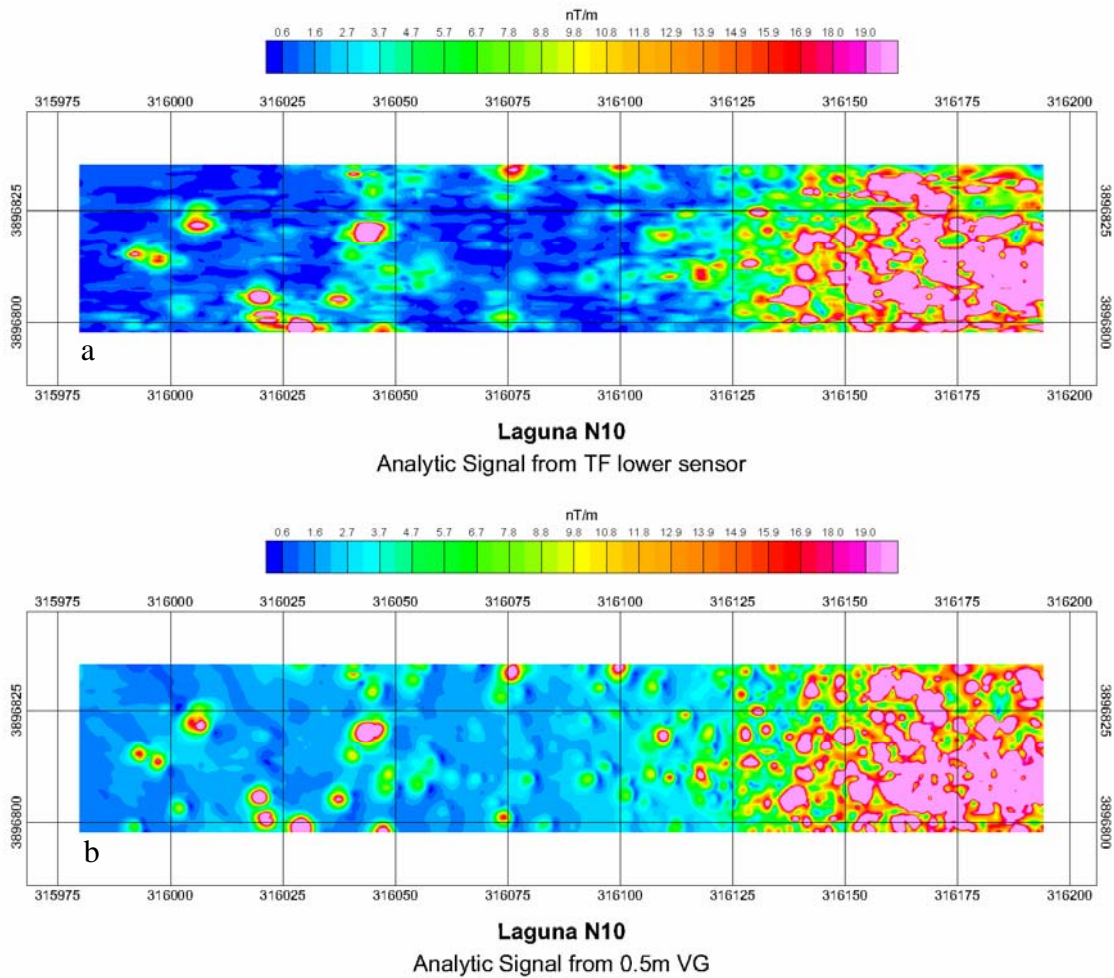


Figure 4-18: Extract of analytic signal map over N-10 bombing target derived from (a) the lower sensor total field data and (b) the vertical gradient data. Background levels adjacent to the strong response of the central target are slightly elevated by the FFT integral calculations.

The results of the Grenade Range survey are shown in Figure 4-19. No excavation was conducted at this site, but several small targets are visible in the analytic signal map. The color scale of the map is set to correspond to the N-10 bombing target for easier comparison.

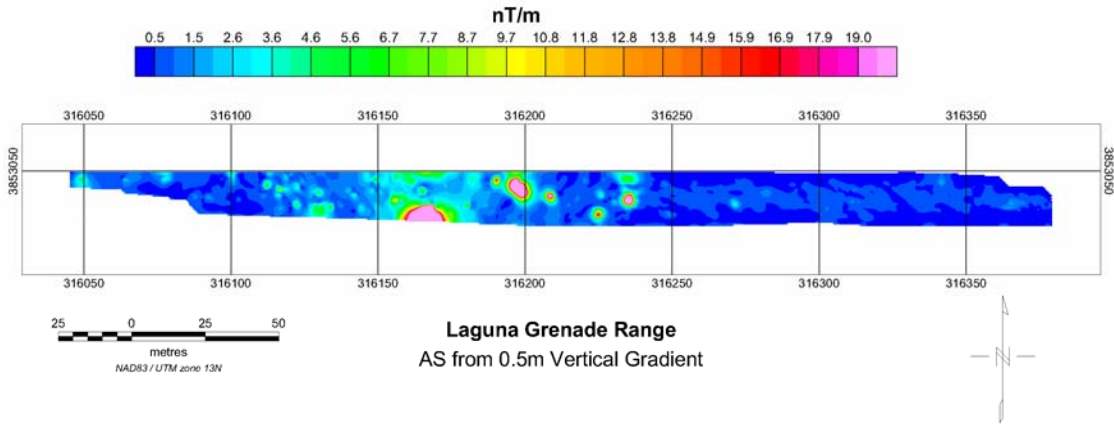


Figure 4-19: Analytic Signal at the Grenade Range derived from the 0.5m vertical gradient data.

### *Field Results – APG*

The Aberdeen Proving Ground site included a calibration grid, a blind seeded grid in a low background noise site (Airfield), and a blind seeded grid in cluttered ground (Mine, Grenade, Direct-fire Weapon Range). For this survey, additional supports were added to stiffen the boom so that the pods would not vibrate. The sample rate for the final data processing was also increased to 120Hz to increase the bandwidth of the data for rotor filtering. The rotor noise examples provided in earlier sections were largely derived from the data collected at this site. All sites were surveyed using the 1m vertical separation and 1m horizontal separation.

The calibration grid included a wide range of ordnance sizes from 60mm to 155mm. This utility of this grid was hampered by a large magnetic anomaly which masked several seeded items. This site was used to calibrate detection thresholds for use in the blind site (Airfield). The dig list was prioritized into 6 categories based on a statistical evaluation of several geophysical parameters. The process was automated except for the “down-selection” of several anomalies clearly attributed to linear cultural features such as fences and roads.

The picking and statistical evaluation process was refined for this site, based on the calibration grid data (Table 4-6). This approach has a significant impact on the final list. The advantages are that local ordnance and geologic settings can be represented. The disadvantages are that the range of seeded ordnance was quite large and it is not known whether these targets were degaussed prior to seeding. Also, the area was not free of debris, which distorted the signatures of the seed items thereby reducing their utility. The cumulative impact on the blind site (Airfield) list is that a larger number of picks were classified as higher priorities than would otherwise be expected in order to encompass the full range of ordnance signatures in the calibration grid.

The picking process was a multi-stage operation. Initial picks were made using the Blakely method applied to the analytic signal (AS) gridded data set. This method compares a grid cell value to adjacent cell values in order to determine peak locations. A second set of picks was made using the Peakedness method, also applied to the analytic signal data. This method compares a grid cell value to a larger radius of neighboring points to determine peak locations. The Blakely method was found to be well suited to detecting anomalies against high amplitude regional trends, whereas the Peakedness method was better suited to selecting targets against low amplitude background noise. The two data sets were then combined into a single list with duplicate picks eliminated.

The picks were then down-selected based on the AS amplitude range found in the calibration grid (1.2-45 nT/m). Picks were further down-selected based on a visual interpretation of linear cultural features such as roads and fences (Airfield only).

The final pick list was divided into 6 categories based on a statistical evaluation of geophysical signature parameters such as apparent depth, amplitude peak separation and dipole orientation. Picks which passed all tests were assigned a priority of 1. Those that passed fewer tests were assigned correspondingly lower priority. As mentioned above, the range of the ordnance and the situation of the calibration grid made it easier for picks at the Airfield site to pass these tests and achieve a higher priority than usual.

When these criteria were assigned to the calibration grid, 33 picks were chosen. Of these, 10 were the seeded items. No seeded items were missed. Seeded items all fell in the top 3 priority categories (6 priority 1, 3 priority 2, 1 priority 3). A complete list of prioritized picks from the calibration grid is presented in Table 4-6. After refining the automated picking process based on known ground truth, a ROC curve was constructed (Figure 4-20). False positive were calculated as the cumulative number of false alarms divided by the cumulative number of picks at each priority level. Gridded data are shown in Figures 4-22 and 4-23.

Applying the same automated procedure to the Airfield data set produced a list with 51 priority 1 picks, 78 priority 2, 54 priority 3 and 76 low priority (4-5-6) picks for a total of 159. A complete list of prioritized targets is provided in Appendix E. From this list, 54 targets were excavated or seeded in conjunction with the total field tests, mostly in priorities 1-3. A ROC curve based on these data was constructed (Figure 4-21). Gridded data are shown in Figure 4-24 and 4-25. These results show a Pd approximately 20% better than any of the total field results with half the false positives (Table 4-5). The system also detected two previously unknown volcano mines in the area which was assumed to be clear. The average location error was 0.87m using a 2m search radius.

Target density over the extract of Mine, Grenade, Direct-fire Weapon Range (MGD) chosen for the vertical gradient was so heavy that no additional analysis could be conducted (Figure 4-26).

Table 4-5: Pd and FP for various detection and discrimination techniques applied to the Airfield site at Aberdeen Proving Ground. UV indicates univariate discrimination, MV is multivariate, and DAS is the MTADS-DAS manual selection method applied to the TF data.

Technique	Pd (% of seeds)	FP (% of digs)
VG (UV)	75%	24%
TF (UV)	54%	48%
TF (MV)	54%	48%
TF (DAS)	56%	49%

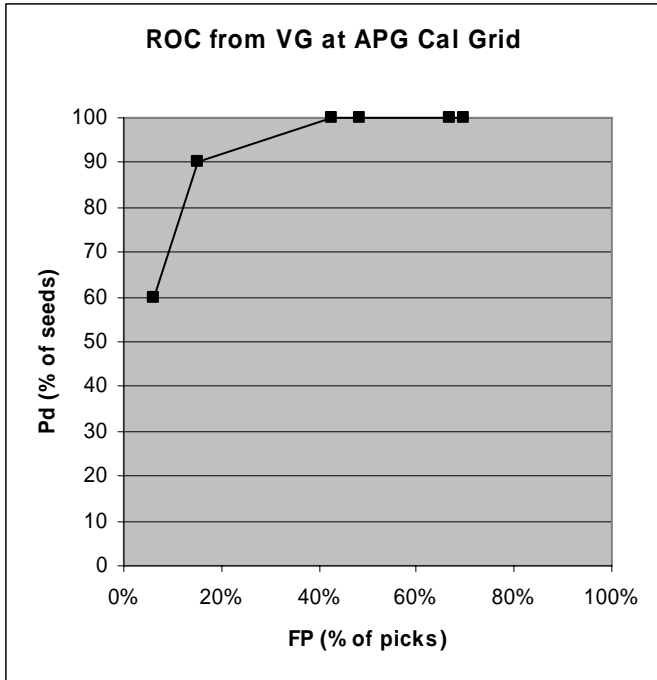


Figure 4-20: ROC curve from APG Calibration Grid using the final automated picking and discrimination routines applied to the vertical gradient data.

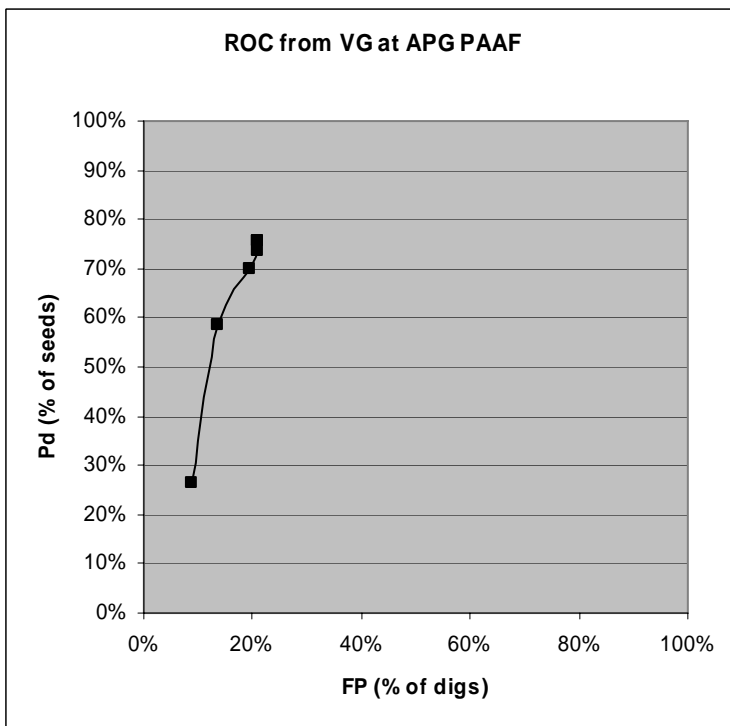


Figure 4-21: ROC curve from APG Airfield using the final automated picking and discrimination routines applied to the vertical gradient data.

Table 4-6: Pick list from APG calibration grid using ORAGS-VG data. XY are in local coordinate projection in meters, AS is analytic signal peak in nT/m. ID numbers correspond to the numbers shown on maps in Figures 4-22 and 4-23.

ID	Priority	X	Y	AS	comment
1	1.00	343.0	625.5	7.362	81mm_seed
2	1.00	336.5	644.5	3.171	60mm_seed
3	1.00	363.5	621.5	3.306	
4	1.00	361.5	622.0	3.773	81mm_seed
5	1.00	381.0	564.3	39.225	155mm_seed
6	1.00	367.5	603.5	14.094	2.75"_seed
7	1.00	362.5	570.0	21.701	155mm_seed
8	1.00	366.8	586.5	16.926	
9	2.00	360.5	616.0	14.366	
10	2.00	359.0	583.5	12.608	
11	2.00	348.5	607.0	1.221	2.75"_seed
12	2.00	357.0	623.0	1.573	
13	2.00	355.5	587.5	8.361	105mm_seed
14	2.00	374.0	585.0	31.897	105mm_seed
15	3.00	358.5	636.0	1.238	
16	3.00	332.5	644.0	1.498	
17	3.00	363.0	631.5	1.497	
18	3.00	347.5	632.0	1.760	
19	3.00	357.0	618.0	3.075	
20	3.00	362.5	574.0	5.076	
21	3.00	362.0	577.5	7.365	
22	3.00	363.0	584.5	9.053	
23	3.00	362.5	616.5	12.182	
24	3.00	355.0	640.5	1.450	60mm_seed
25	4.00	350.0	654.0	1.287	
26	4.00	339.5	650.5	1.383	
27	5.00	380.5	567.5	13.822	
28	5.00	356.5	643.5	1.291	
29	5.00	346.0	638.0	1.216	
30	5.00	351.5	639.5	1.315	
31	5.00	339.5	645.0	1.588	
32	5.00	335.0	629.5	1.251	
33	6.00	336.0	639.5	1.312	

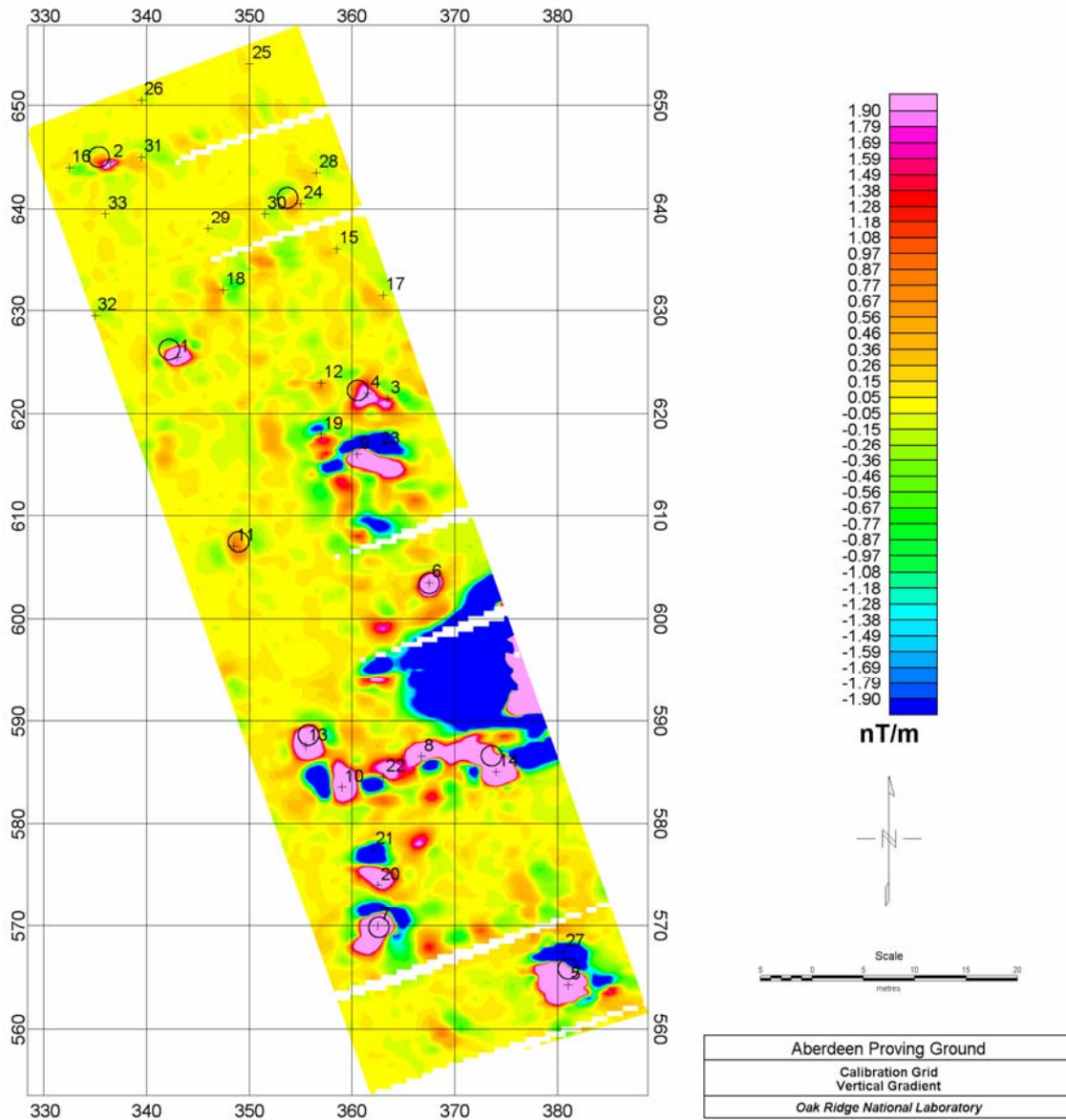


Figure 4-22: Vertical Gradient map over the APG Calibration Grid. Seeded items are presented as circles, picked anomalies as numbered crosses.

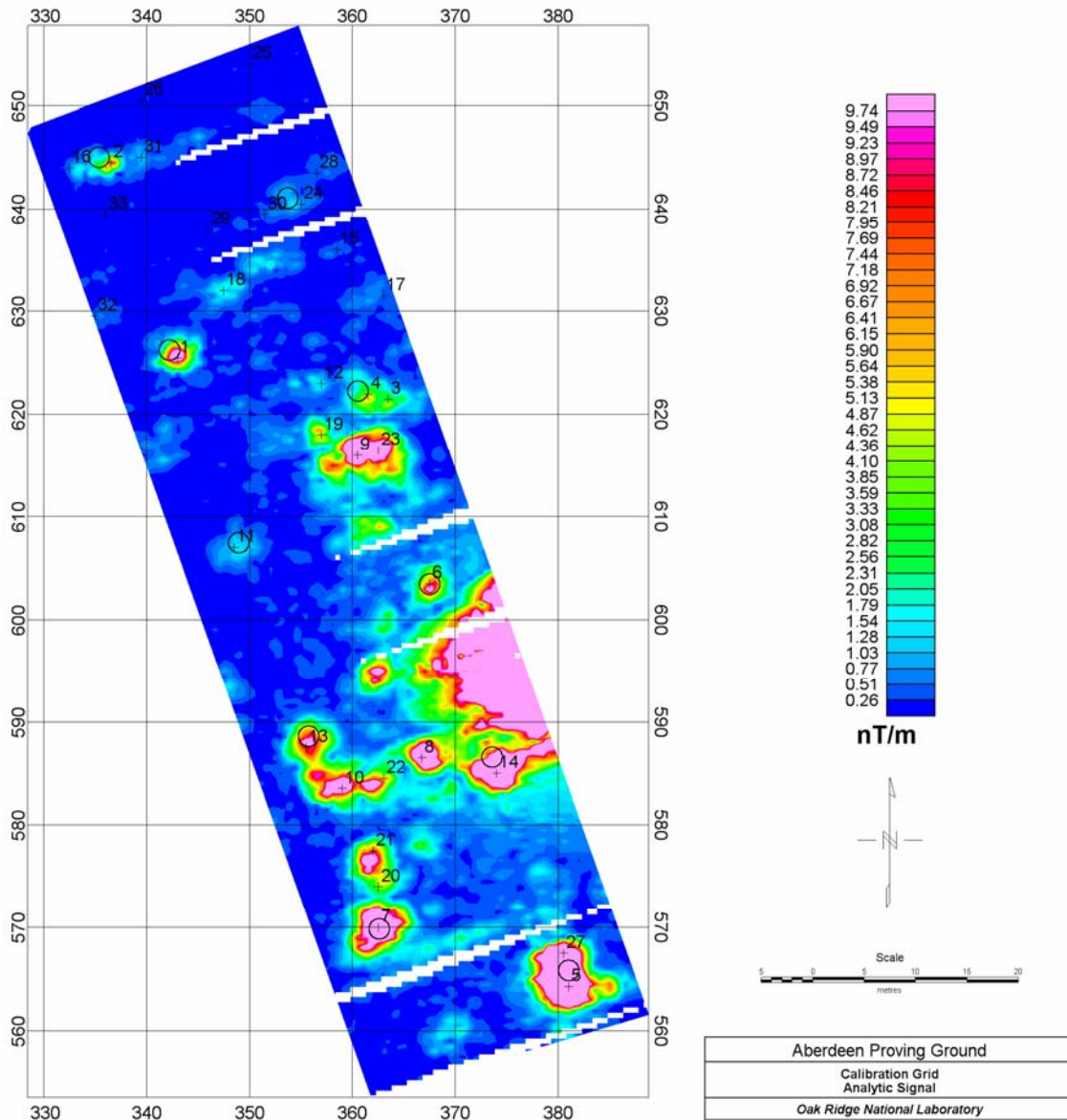


Figure 4-23: Analytic Signal map over the APG Calibration Grid derived from the vertical gradient. Seeded items are presented as circles, picked anomalies as numbered crosses.

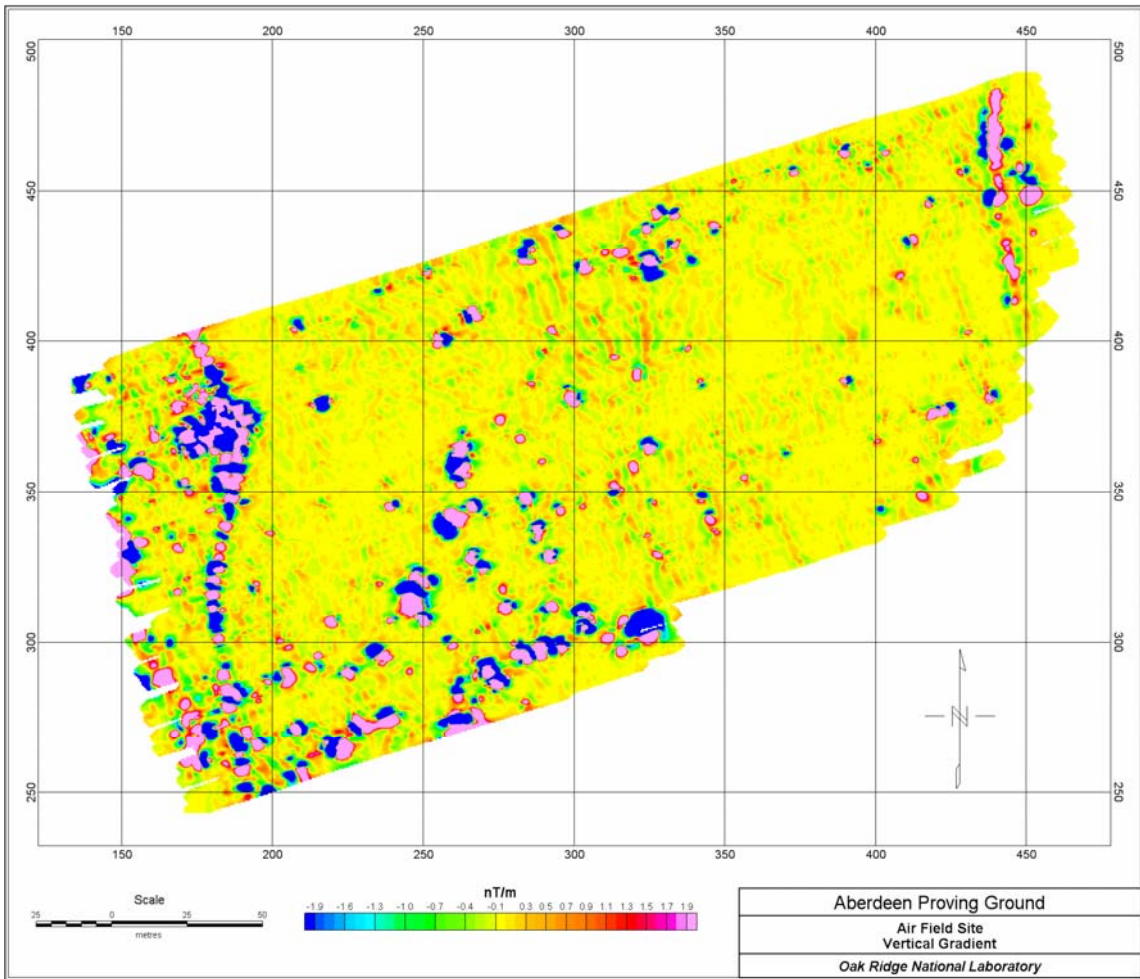


Figure 4-24: Vertical gradient map of the APG Airfield site.

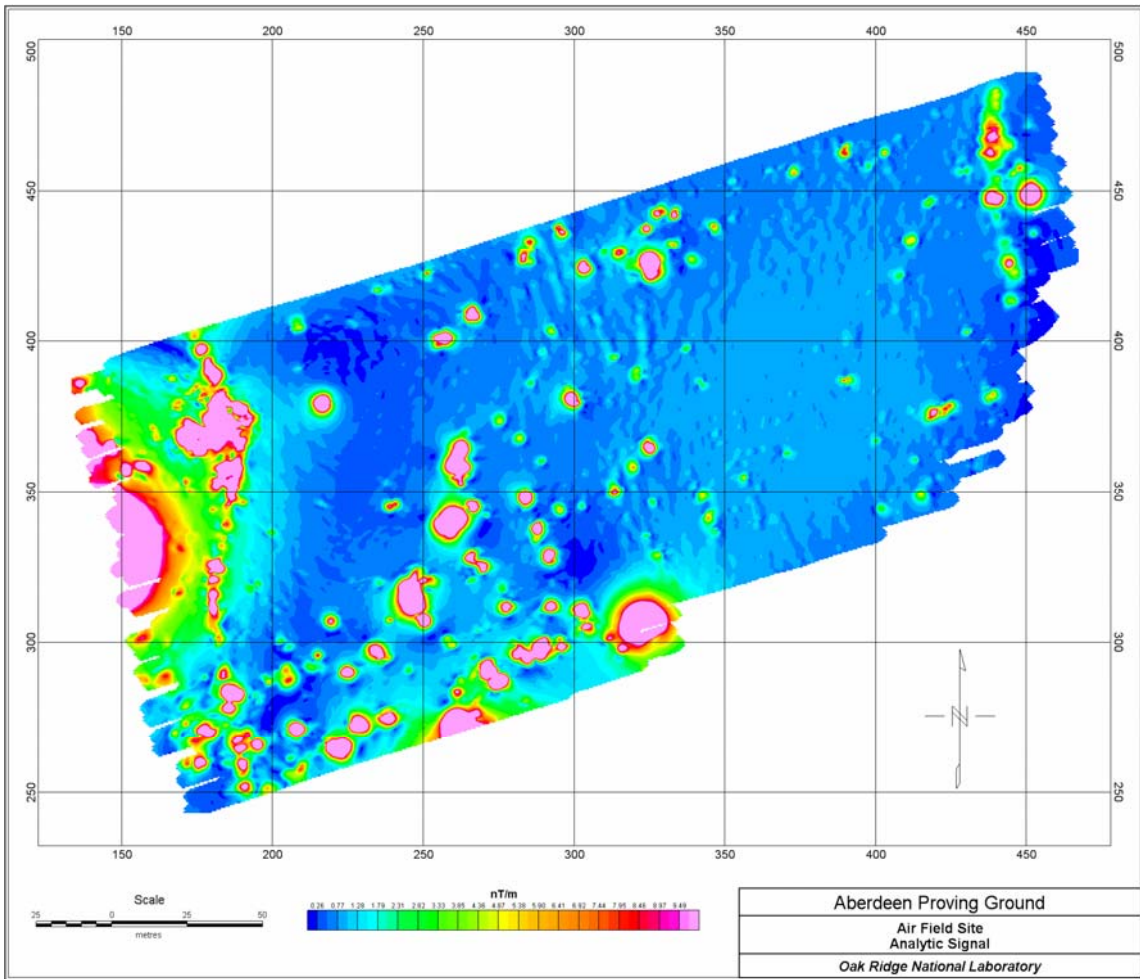


Figure 4-25: Analytic Signal derived from the vertical gradient at the APG Airfield site.

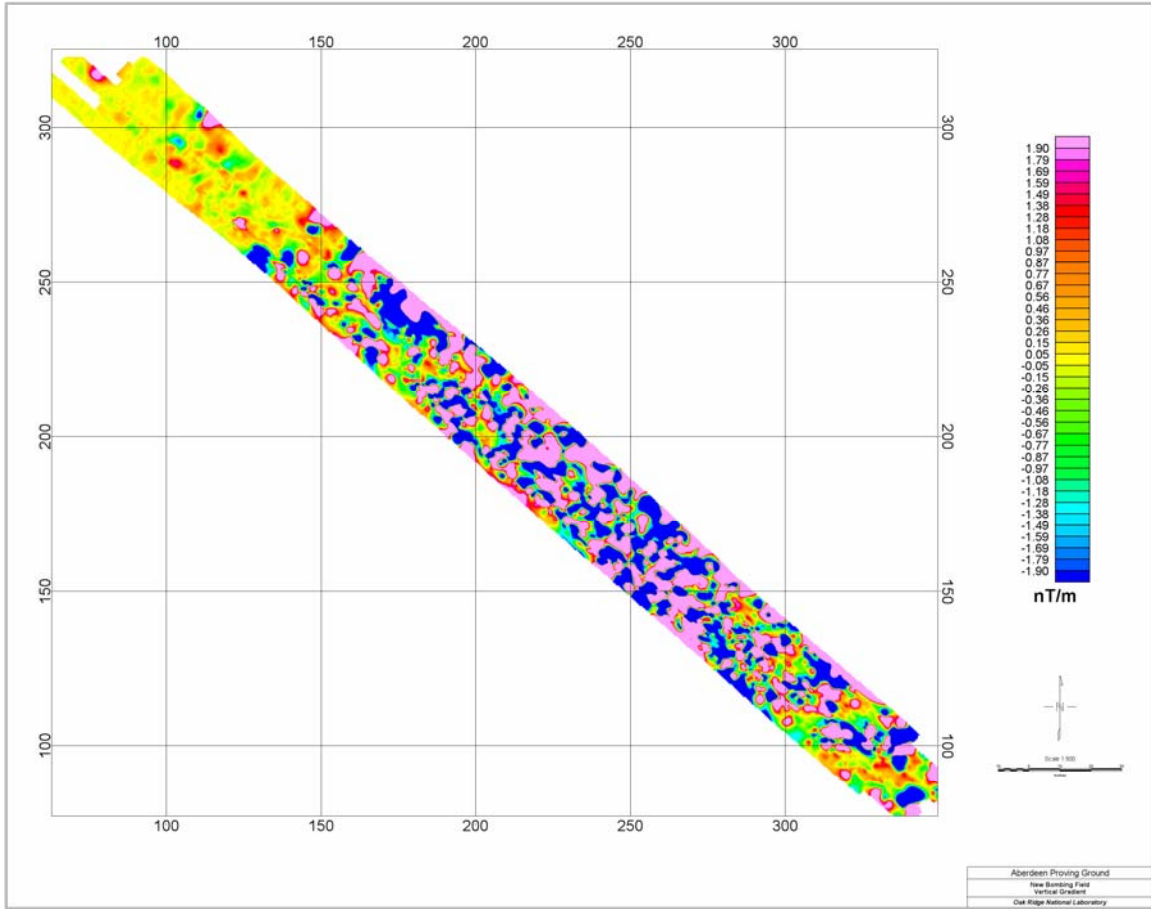


Figure 4-26: Vertical gradient map of a section of the APG Mine, Grenade, Direct-fire Weapon Range.

### *Field Results – BBR*

The Badlands Bombing Range includes several bombing targets within the Oglala Sioux Reservation in South Dakota. The Calibration Grid is located in the north central section of Cuny Table. Bombing Target 1 (BT-1) is located in the western section of Cuny Table.

The data sets used to analyze the rotor noise were drawn principally from this survey. In particular, the three small UXO targets shown in Figure 4-6 and Table 4-3 are from the BBR Calibration Grid. The clustered targets shown in Figure 4-11 are from BT-1.

The BBR site consisted of a calibration grid and a partially remediated bombing target. The calibration grid measured 105m x 150m with 52 seeded items. These test items include several types of inert ordnance as well as a number of pipes and other hardware items (Table 4-7). It was intended that the test site include some items that would be too small to be detected by some or all of our systems. Some positions in the grid were unoccupied because they were previously used for surface test objects that were subsequently removed. Their depth of burial, orientation, and length are found in Beard et al., 2004, and other references. The masses of the objects range from less than 1 kg to more than 50 kg, and depth of burial ranges between 0 and 1.3m.

The second site at BBR was designated Bombing Target 1. This site has been used for several ground and airborne demonstrations and has been partially remediated. The target is divided almost evenly into northern and southern halves by a barbed wire fence. The land on the south side is under cultivation while the land on the north side is range land for livestock. The majority of the ordnance at this location are M38 sand-filled practice bombs.

Figures 4-27 through 4-31 show the entire survey blocks for the Calibration Grid and Bombing Target-1.

The analysis of the system performance was focused on the aerodynamic stability, the compensation and rotor noise reduction capabilities of the system, and a qualitative assessment of its detection performance. This performance analysis has been presented in sections 4.3.2, 4.3.3, and 4.3.7. No excavations of this area were planned or carried out. The exact locations of the test grid objects were also suspect, as they had been shifted by freeze-thaw over several years.

ID	Description	Mass (kg)
<b>Row A</b>		
A1	8 in nail+2 in galv pipe	2.7
A2	3 rebar rods	5.5
A3	2 in galv pipe elbow	4.5
A4	steel channel	6.8
A5	2 in galv pipe	2.7
A6	2 in galv pipe with flanges	4.5
A7	unknown	
A8	box beam	4.5
A9	galv stove pipe	1.8
A10	8 in nail	
<b>Row B</b>		
B1	I beam	13.2
B2	4 rebar rods	4.1
B3	I beam	4.5
B4	250 lb bomb	52
B5	100 lb bomb fragments	unk
<b>Row C</b>		
C1	100 lb bomb fragments	8.6
C2	250 lb bomb simulant	22.7
C3	250 lb bomb simulant	29
C4	100 lb bomb intact	22.7
C5	100 lb bomb fragments	14.5
C6	2.75 in rocket nose section	4.1
C7	155 mm round	24
C8	105 mm round	8.6

Table 4-7: Items buried at the BBR Calibration Site.

ID	Description	Mass (kg)
<b>Row D</b>		
D1	100 lb bomb fragments	unk
D2	100 lb bomb fragments	unk
D3	2.75 in rocket cylinder	4.1
D4	2.75 in rocket	2.3
D5	105 mm round	8.6
D6	2 2.75 in rocket sim.	5.4
D7	61 mm mortar	0.9
D8	105 mm round	8.6
<b>Row E</b>		
E1	81 mm round	4.1
E2	aluminum rod	0.5
E3	aluminum rod	0.5
E4	aluminum rod	0.5
E5	81 mm round	3.6
E6	81 mm round	3.6
E7	105 mm round	8.2
<b>Row F</b>		
F1	81 mm round	3.2
F2	60 mm illum. round	1.8
F3	60 mm illum. round	1.8
F4	60 mm illum. round	0.9
<b>Row G</b>		
G1	81 mm round	3.2
G2	100 lb bomb	2.7
G3	60 mm mortar round	1.4
G4	2.25 in rocket	4.5
G5	steel pipe	4.1
<b>Row H</b>		
H1	8 in nail	
H2	2.75 in rocket	3.2
H3	155 mm round	25.5
H4	155 mm round	25.5
H5	155 mm round	25.5
H6	8 in nail	

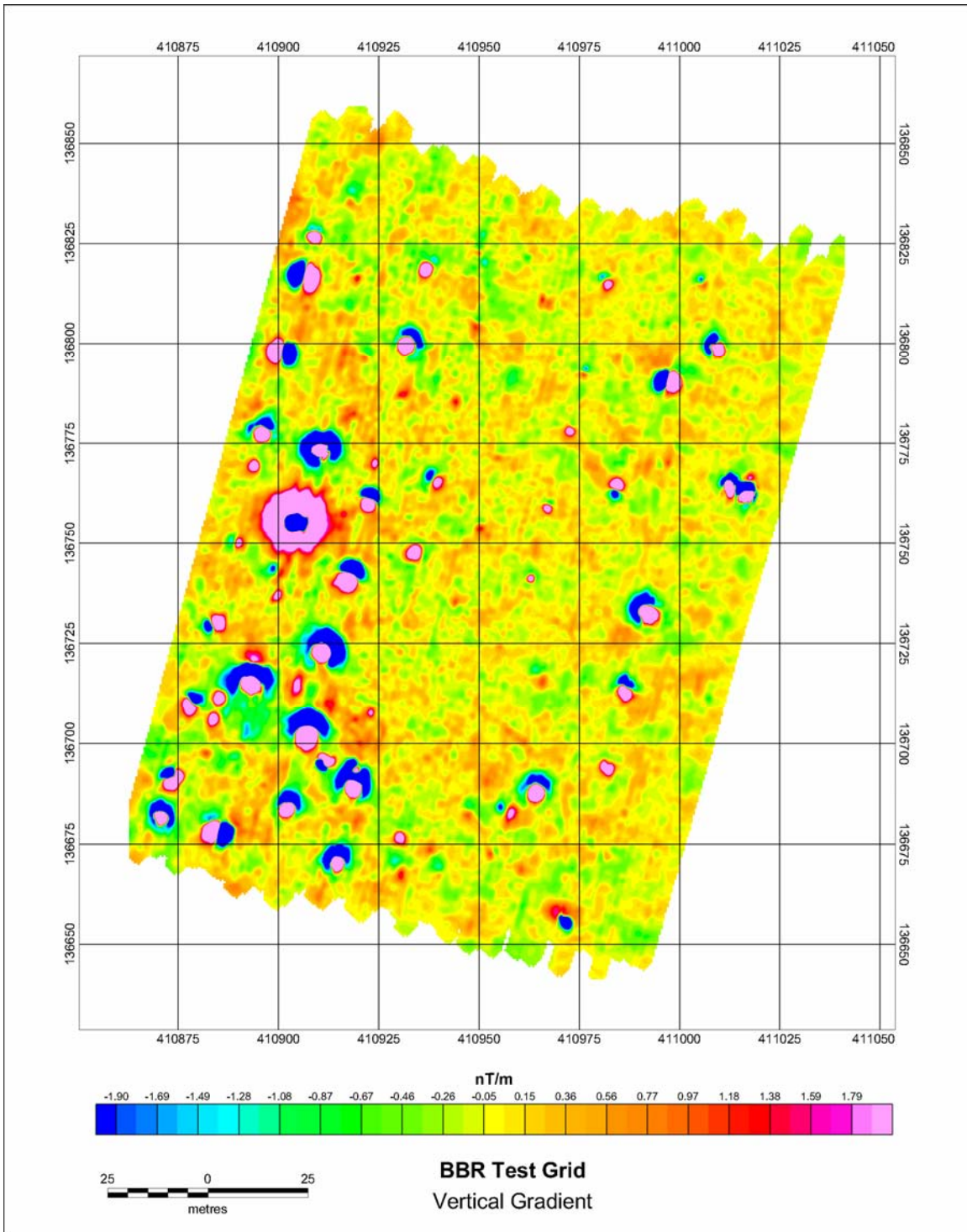


Figure 4-27: Vertical gradient response over the BBR Test Grid. Survey parameters included 1m survey height with 1m vertical sensor separation and 1m horizontal sensor separation

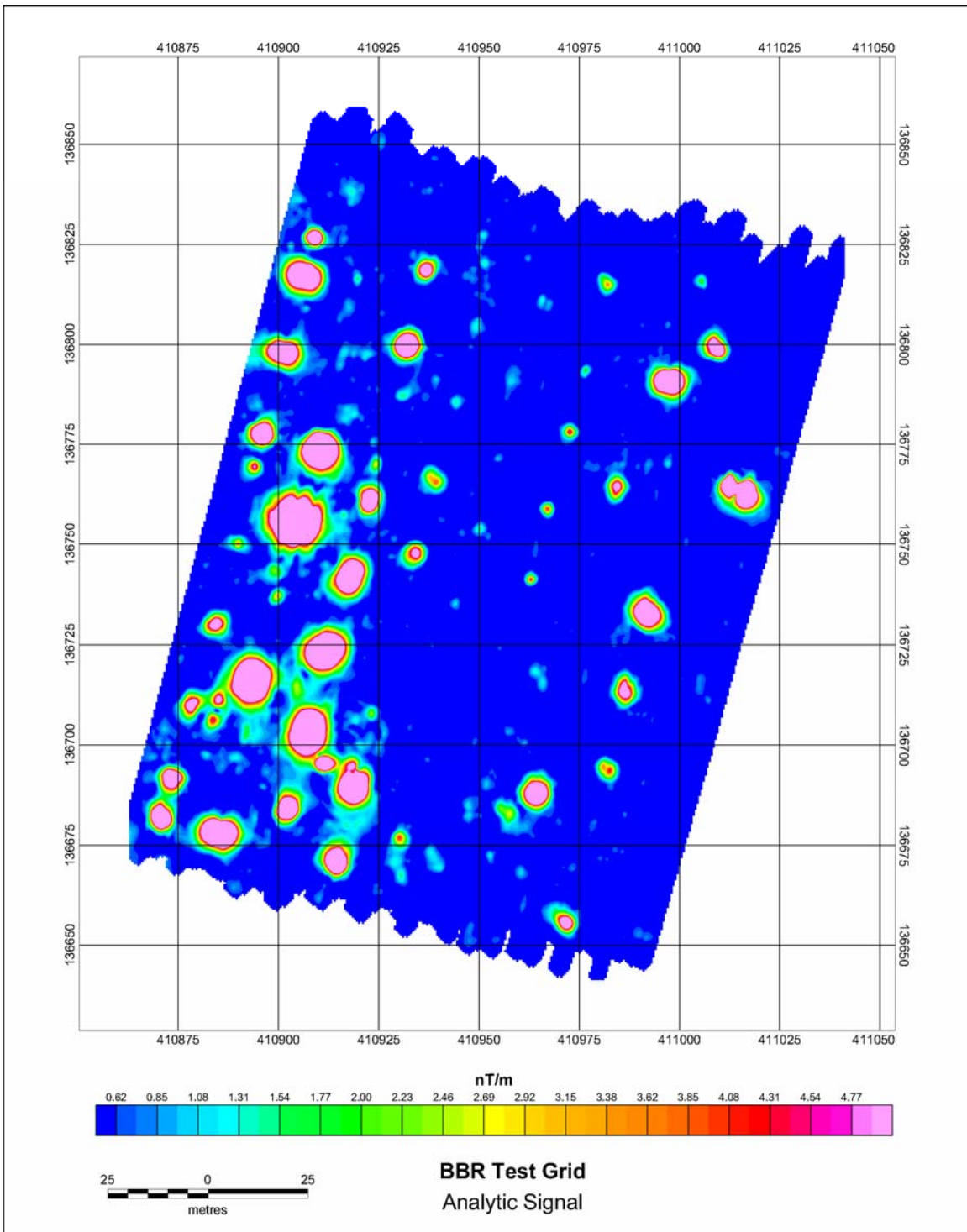


Figure 4-28: Analytic signal response over the BBR Test Grid as derived from the vertical gradient data in Figure 4-27.

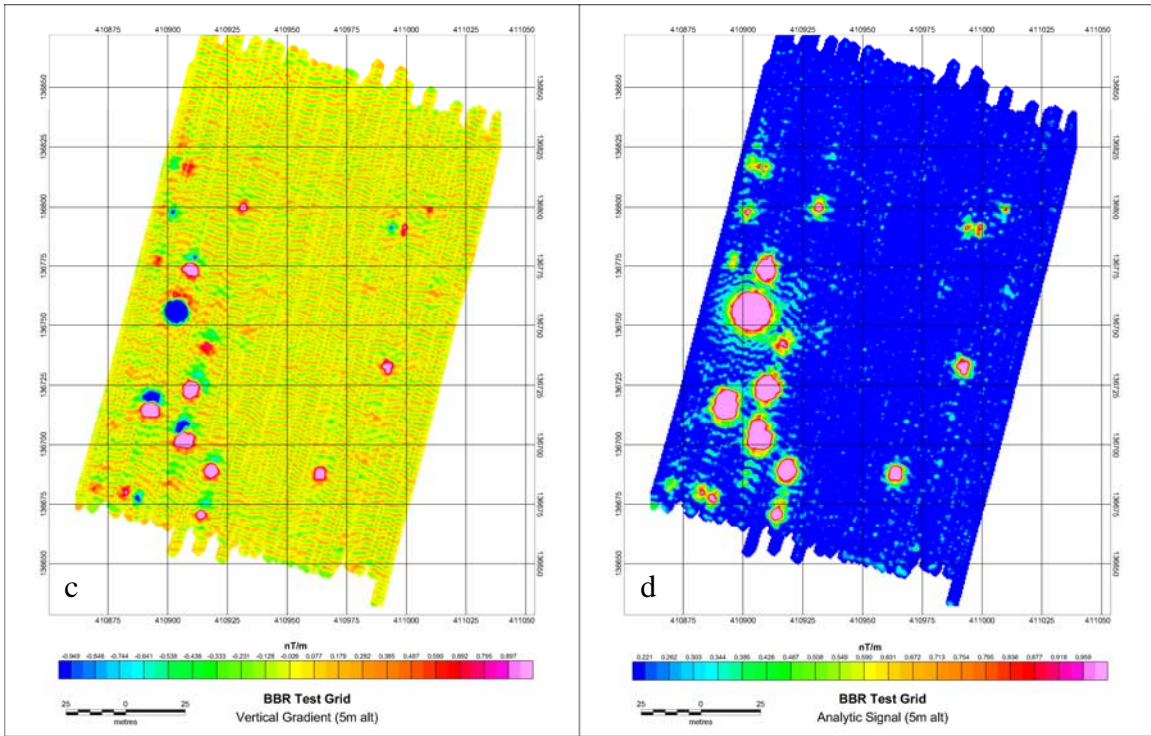
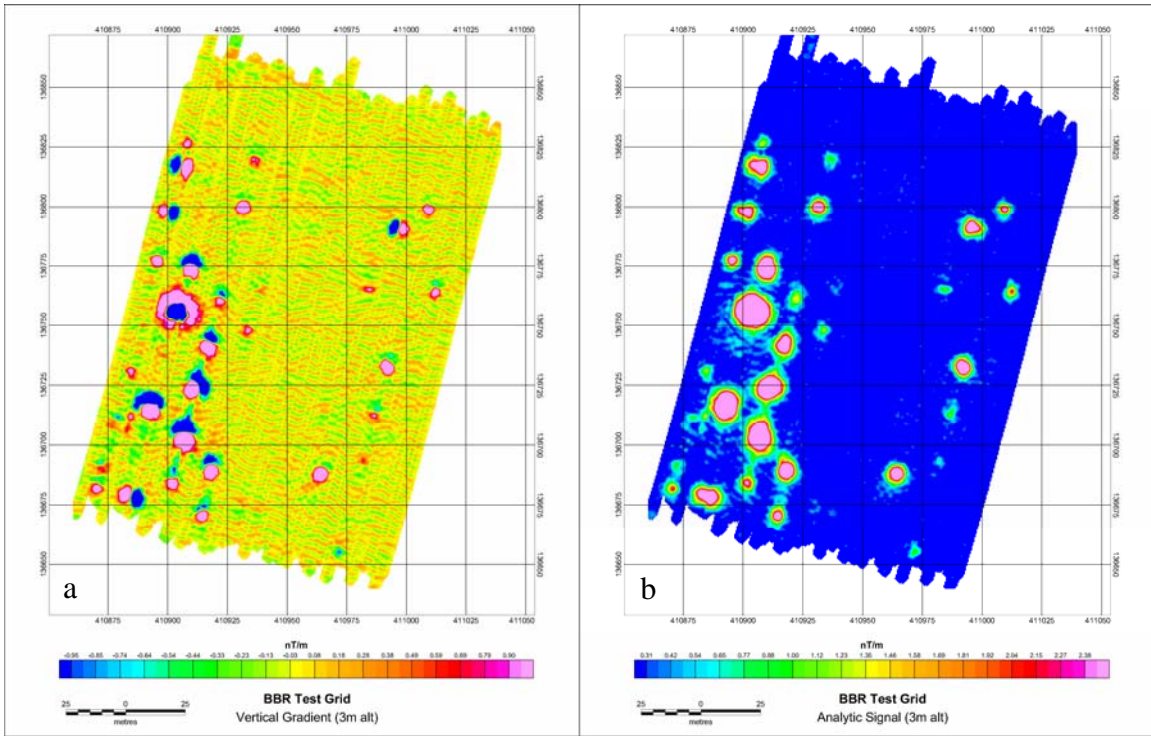


Figure 4-29: BBR Test Grid data from (a, b) 3m and (c, d) 5m survey altitudes. The wavy noise in the grids are the result of spatially-coherent low-amplitude remnants of rotor noise which is now visible with the finer color contours.

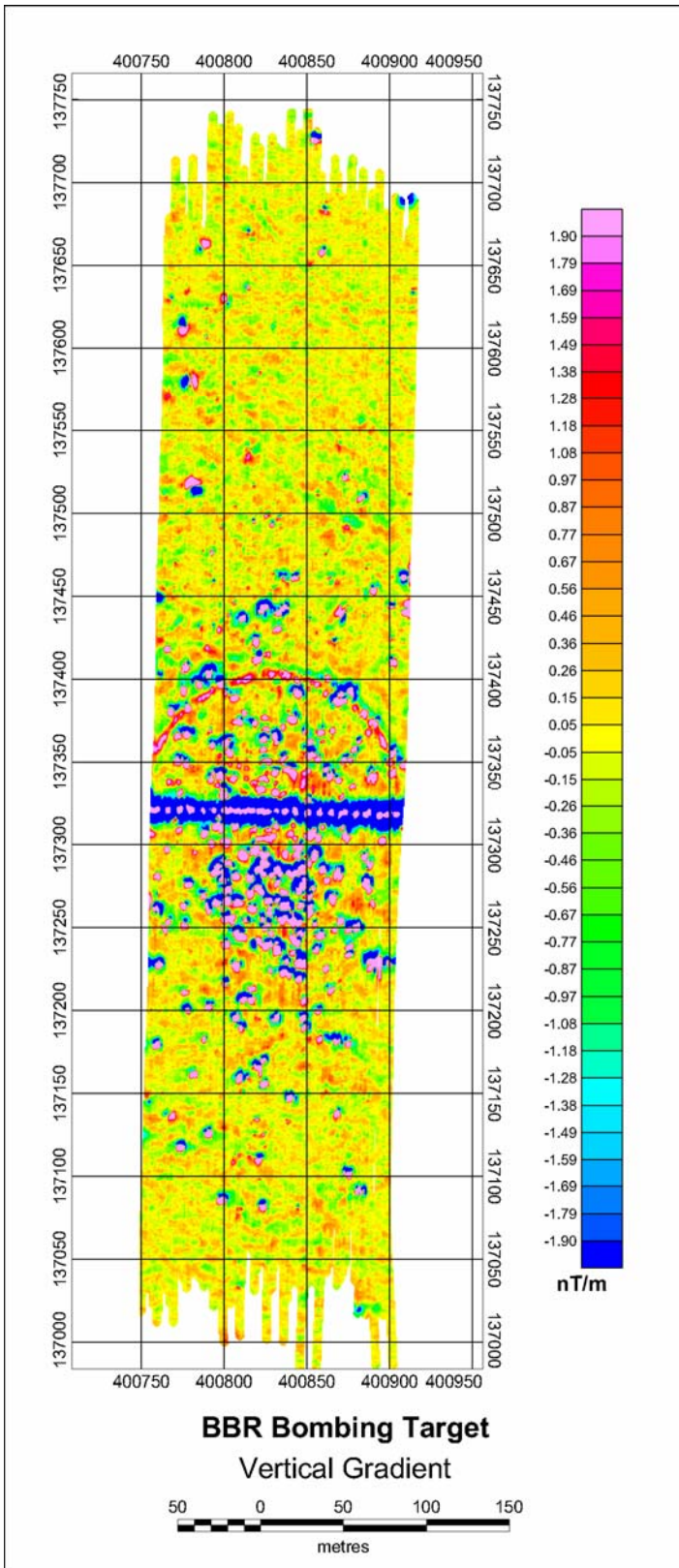


Figure 4-30: Vertical gradient response over Bombing Target 1. Survey parameters include 1.5m survey height, 1m vertical sensor separation, 1m horizontal separation.

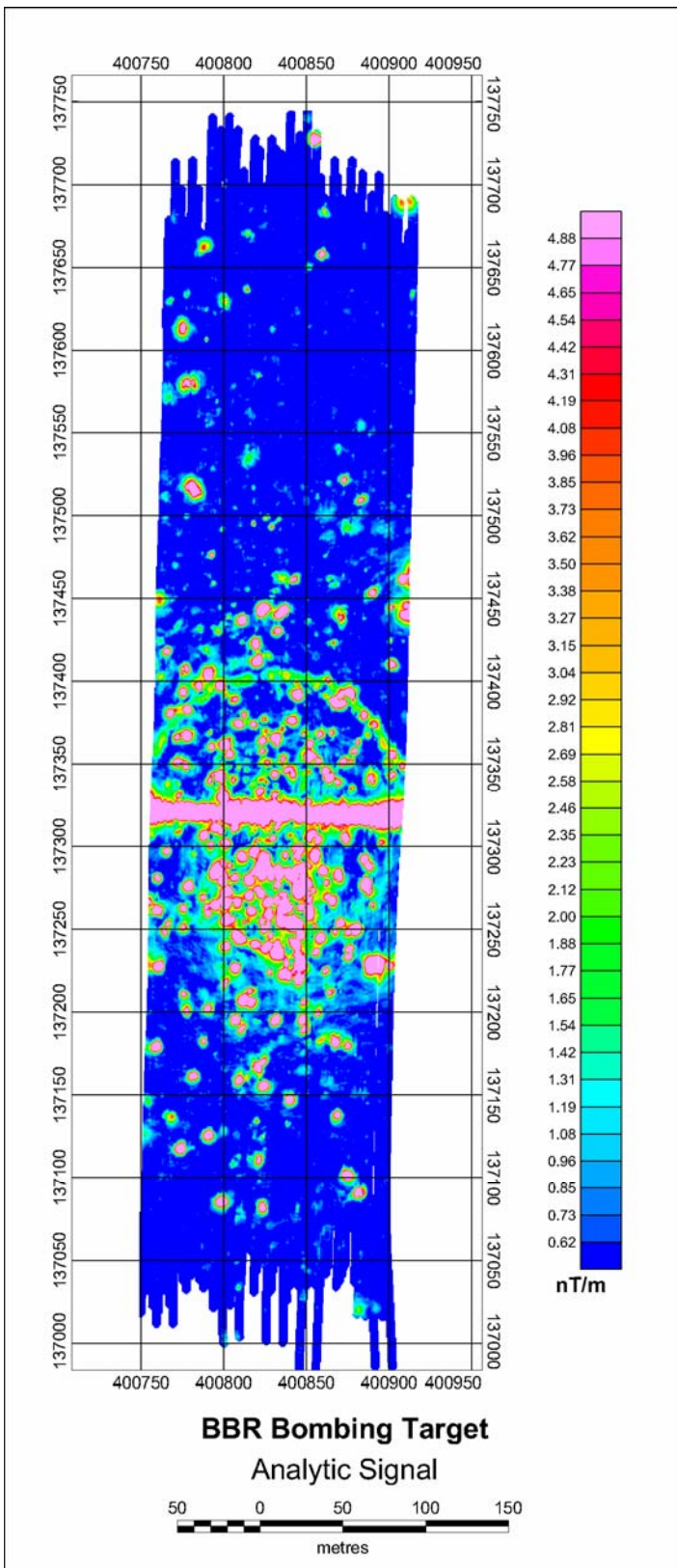


Figure 4-31: Analytic signal response over Bombing Target 1 derived from vertical gradient data in Figure 4-30.

### 4.3.9 Recommendations for design modifications

The second objective of this demonstration (sec 1.2) is to recommend design modifications for a production vertical gradient system. The foregoing analysis was conducted using a prototype system that included only four gradient pairs which required considerable interleaving to achieve full coverage. The practical benefits of the vertical gradient system have been demonstrated as the ability to detect objects roughly five times smaller (smaller magnetic moment) than the total field system, or to detect them at approximately 1.5m greater altitude. From a system design perspective, these two objectives represent two different configurations. In preparation for development of a production system that does not require interleaving, this section details some of the design implications arising from the study of the data.

The vertical gradient configuration eliminates a significant portion of the helicopter noise related to both maneuvering (six times improvement) and rotors (four times improvement). The noise still increases with proximity to the aircraft, however. Regardless of the survey objective, sensors should still be mounted as far from the body of the helicopter as possible.

A dipole signature from a typical UXO target has also been shown to be roughly half as wide as a total field signature. This implies that sensor pairs should be mounted closer together than in the total field configuration to avoid having targets fall between sensor traces. This is particularly true if the objective is detection of very small targets (smaller than 81mm) from very low altitudes (<2m). The 1m horizontal spacing on the data from the BBR Test Grid clearly shows the small targets such as the 60mm illumination rounds (Figure 4-32a). Desampling the data to alternate lines (2m) shows that the targets are captured only if the sensor passes directly over it (Figure 4-32b). Using the “other” set of alternate lines where the target falls between the sensor traces (Figure 4-32c) clearly demonstrates a missed target. A design specification of 1m horizontal sensor spacing is recommended for this application.

The effects of a narrower gradient signature are offset when higher survey altitudes are used. The additional height broadens the spatial extent of the signature, thereby eliminating the requirement for closer line spacing (Figure 4-33).

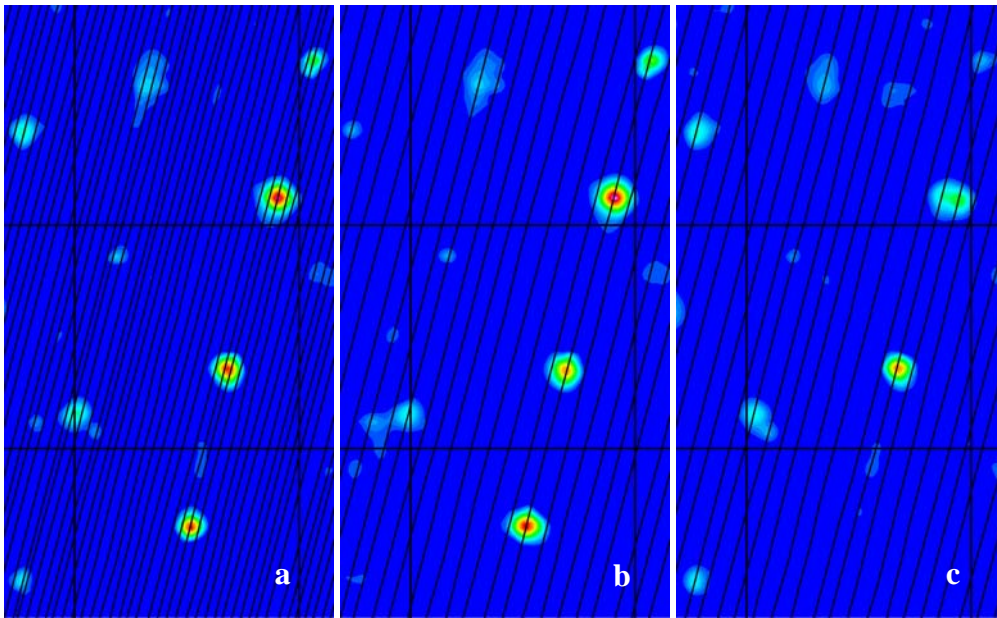


Figure 4-32: Extract of analytic signal data from BBR Test Grid at 1m survey altitude (25m reference grid, color scale as per original Figure 4-28). (a) original 1m line spacing (b) odd number lines to represent 2m line spacing (c) even number lines. Note how small targets may be lost with inadequate line spacing.

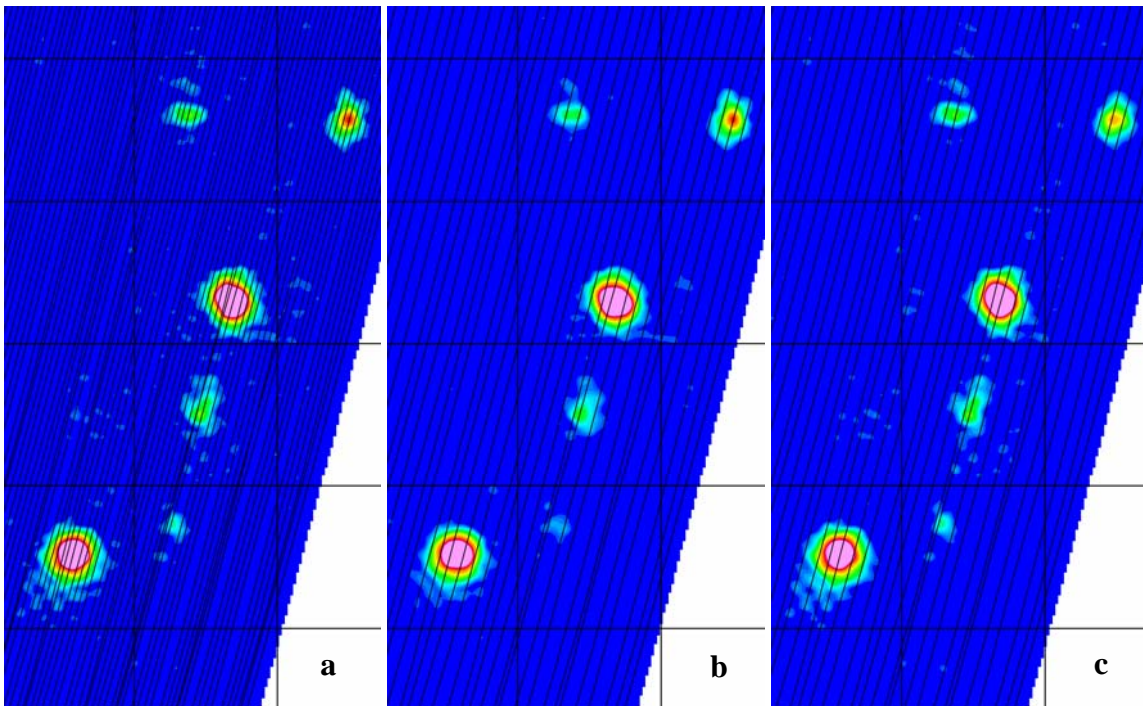


Figure 4-33: Extract of analytic signal data from BBR Test Grid at 3m survey altitude (25m reference grid, color scale as per original Figure 4-29). (a) original 1m line spacing (b) odd number lines to represent 2m line spacing (c) even number lines. Even though very small targets are below the detection threshold, those that are detectable are broad enough to be detected at the wider line spacing.

The conclusion to this analysis is that a production version of the vertical gradient system should be developed. This system should be adaptable in order to address different survey objectives. The two primary strengths of the vertical gradient system are the ability to detect UXO at greater survey heights, and the ability to detect smaller objects at lower survey heights. Where higher altitudes are required, the current 12m swath with a 1.7m sensor spacing is appropriate. This would involve mounting gradient pods at roughly the same locations as the current total field sensors. The additional weight in the forward boom may require a small amount of ballast, but should not hamper overall aerodynamics.

Where lower altitudes are practical, an option for narrower sensors spacing will be required. Using the existing boom structure as a starting point, eight pairs of gradient pods could be mounted on the forward boom at approximately 0.9m intervals. This would present a narrower swath, and would require ballast and twice as many lines per acre. The lateral booms should be retained in this configuration for aerodynamic stability and as mounting locations for the orientation sensors.

## **5 Cost Assessment**

### **5.1 Cost Reporting**

Cost information associated with the demonstration of the vertical magnetic gradient airborne technology, as well as associated activities, were closely tracked and documented before, during, and after the demonstration to provide a basis for determination of the operational costs associated with this technology. It is important to note that the costs for airborne demonstrations and surveys are very much dependent on the character, size, and conditions at each site; ordnance objectives of the survey (e.g. flight altitude); type of survey conducted (e.g. high-density or transects); and technology employed for the survey (e.g. total field magnetic, vertical magnetic gradient, time domain electromagnetic induction) so that a universal formula cannot be fully developed. For this demonstration, the following table contains the cost elements that were tracked and documented for this demonstration. These costs include both operational and capital costs associated with system design and construction; salary and travel costs for support staff; subcontract costs associated with helicopter services, support personnel, and leased equipment; costs associated with the processing, analysis, comparison, and interpretation of airborne results generated by this demonstration. All of the vertical gradient surveys were conducted in conjunction with total field surveys at the same site. Mobilization costs are reported in the associated ORAGS-Arrowhead project reports and are not duplicated here.

<b>Cost Category</b>	<b>Sub Category</b>	<b>Details</b>	<b>Quantity</b>	<b>Cost<sup>1</sup> (in dollars)</b>
Pre-Survey (Start-up)	Site Characterization	Site inspection:		
		Aberdeen, MD (APG)	0 days	\$0
		Albuquerque, NM (Laguna)	0 days	\$0
		Pine Ridge, SD (BBR)	0 days	\$0
		Mission Plan preparation & logistics (majority of effort covered under corresponding APG, Laguna, and BBR survey projects)	3 days	\$5,307
		Calibration Site development <sup>2</sup> (includes pre-seed and post-seed ground-based surveys) at the following sites:		
		Aberdeen, MD	0 days	\$0
	Albuquerque, NM	0.5 day	\$1,655	
	Pine Ridge, SD	0 days	\$0	
	Mobilization	Equipment/personnel transport (includes travel):		
Aberdeen, MD		0 days	\$0	
Albuquerque, NM		0 days	\$0	
Pine Ridge, SD		0 days	\$0	

Pre-Survey (cont'd)		Helicopter/personnel transport <sup>3</sup> (includes travel):		
		Aberdeen, MD	0 days	\$0
		Albuquerque, NM	0 days	\$0
		Pine Ridge, SD	0 days	\$0
		Unpacking and system installation:		
		Aberdeen, MD	1 day	\$4,559
		Albuquerque, NM	1 day	\$4,559
		Pine Ridge, SD	1 day	\$4,559
		System testing & calibration:		
		Aberdeen, MD	1 day	\$6,309
	Albuquerque, NM	1 day	\$6,572	
	Pine Ridge, SD	1 day	\$6,747	
Pre-survey subtotal				\$40,267

System Development & Capital Equipment <sup>4</sup>	Cesium-vapor magnetometers	\$122,200 total cost	8 each	\$0
	GPS	\$15,500 total cost	1 each	\$0
	Booms and mounting hardware	\$36,500 total cost	1 set	\$0
	Pods and mounting hardware	\$12,500 total cost	1 set	\$12,500
	Orientation system	\$16,600 total cost	1 each	\$0
	Fluxgate magnetometer	\$5,300 total cost	1 each	\$0
	Navigation system	\$5,200 total cost	1 each	\$0
	Laser Altimeter	\$7,300 total cost	1 each	\$0
	Data management console	\$31,200 total cost	1 each	\$0
	Magnetic base station	\$15,100 total cost	1 each	\$0
	GPS base station	\$15,600 total cost	1 each	\$0
	PCs for data processing & analysis	\$3,450 total cost	2 each	\$0
	Shipping Cases	\$4,750 total cost	6 each	\$0
	Trailer	\$3,600 total cost	1 each	\$0
Capital subtotal				\$12,500

Operating Costs (includes Aberdeen, Albuquerque, and Pine Ridge)	Equipment Rental <sup>3</sup>	Spare magnetometers	2 each	\$0
		GPS equipment	1 each	\$0
	Data acquisition	Helicopter time, including pilot and engineer labor	7 days (31 hours airborne)	\$24,800
	Operator labor		7 days	\$1,225
	Data processing	Geophysicist	8 days (40 hours labor)	\$12,320
	Field support/management	Engineer	8 days (40 hours labor)	\$12,320
	Maintenance	Geosoft software maintenance <sup>3</sup>	1 each	\$0
	Hotel and per diem	Survey team	8 days	\$4,016
	Fuel Truck	Remote re-fueling <sup>3</sup>	-	\$0
	Airport Landing Fees		7 days	\$175
	Data analysis and interpretation	Geophysicist	10 days	\$15,446
	Project management		4 days	\$6,164
	Reporting and documentation		10 days	\$15,460
Operating cost subtotal				\$91,926

Post-Survey	Demobilization	Disassembly from helicopter, packing, and loading for transport:		
		Aberdeen, MD	1 day	\$4,559
		Albuquerque, NM	1 day	\$4,559
		Pine Ridge, SD	1 day	\$4,559
		Equipment/personnel transport <sup>3</sup> (includes travel):		
		Aberdeen, MD	0 days	\$0
		Albuquerque, NM	0 days	\$0
		Pine Ridge, SD	0 days	\$0
		Helicopter/personnel transport <sup>3</sup> (includes travel):		
		Aberdeen, MD	0 days	\$0
Albuquerque, NM	0 days	\$0		
Pine Ridge, SD	0 days	\$0		
Post-survey subtotal				\$13,667
Miscellaneous	Department of Energy Federal Acquisition Cost (FAC)	3% of project total; Congressionally-mandated charge for administering the Work-for-Others (WFO) program		\$4,751
Total costs				\$163,111

<sup>1</sup>**Includes all overhead and organization burden, fees, and associated taxes**

<sup>2</sup>**No significant costs were incurred for the establishment of Calibration Sites at any of the demonstration sites. Existing sites established under previous survey projects were used for system testing and development**

<sup>3</sup>**These costs were included in related airborne magnetic survey projects occurring in conjunction with vertical magnetic gradient system testing and development (leveraged costs)**

<sup>4</sup>**Capital costs associated with airborne system components and related equipment (except the pods and mounting hardware) were acquired under other projects (e.g. development of airborne magnetic system) and are not included in the cost of this project (leveraged cost)**

## **6 Implementation Issues**

### **6.1 Environmental Checklist**

In order to operate, each system must have Federal Aviation Administration approval (STC certificate). The required testing and evaluation was completed before mobilization. In addition, ground crews are required to complete the 40-hour HAZWOPR course and to maintain their annual 8-hour refreshers for operation at most UXO sites.

### **6.2 Other Regulatory Issues**

Security clearance for the aircraft equipment and personnel was required at the APG site. Specific entry and exit flight corridors were also established at this site. There were no additional regulatory requirements for operation at either of the other two sites.

### **6.3 End-User Issues**

The primary stakeholders for UXO issues at the Laguna site in New Mexico are the members of the Pueblo of Laguna Nation, other residents of Pueblo of Laguna Reservation, and State of New Mexico regulatory authorities. Similar stakeholders were identified within the Oglala Sioux Nation at BBR in South Dakota. At APG, the DoD and its associated agencies with responsibilities at the site represented the primary stakeholders.

The vertical gradient technology used here is a prototype derived from the ORAGS-Arrowhead system. Scale up will require additional booms and sensors to create a production system which does not require interleaving of lines. Sufficient electronics and recording systems are already available for this production system. As such, this system is not yet ready for commercial operations on a larger scale. As the system is developed and proven, it will enter into the same cycle of application and commercialization as the total field system.

## 7 References

- Breiner, S., 1973, Applications manual for portable magnetometers, GeoMetrics, 58p.
- Doll, W.E., T.J. Gamey, L.P. Beard, A.M. Emond, D.T. Bell, 2004, Comparison of airborne vertical magnetic gradient and total field products for mapping and detection of UXO and ferrous wastes, 74th Ann. International Meeting: Society of Exploration Geophysics, Session: GM3. (in publication).
- Doll, W.E., T.J. Gamey, L.P. Beard, D.T. Bell, and J.S. Holladay, 2003, Recent advances in airborne survey technology yield performance approaching ground-based surveys, *The Leading Edge*, v. 22, n. 5, p. 420-425.
- Doll, W.E., L.P. Beard, and T.J. Gamey, 2002, An advanced airborne magnetic system for high-resolution mapping, *Expanded Abstracts, Society of Exploration Geophysicists Annual Meeting, Salt Lake City, Utah, October 6-11, 2002*, 4 pp., available on CD-ROM.
- Gamey, T.J., W.E. Doll, L.P. Beard, D.T. Bell, 2004, Analysis of Correlated Noise in Airborne Magnetic Gradients for UXO Detection, *Journal of Environmental and Engineering Geophysics*, (in publication).
- Gamey, T.J., W.E. Doll, L.P. Beard, D.T. Bell, 2003, Airborne Geophysics for Shallow Object Detection: Technology Update 2003 – Magnetics, Proceedings of Ninth European Meeting of EEGS (abstract), Prague.
- Gamey, T.J. and R. Mahler, 1999, A comparison of towed and mounted helicopter magnetometer systems for UXO Detection, Extended Abstract in *Proceedings of the 1999 SAGEEP Symposium*, p. 783-792.
- Hardwick, C.D., 1986, Techniques for achieving stable and robust aeromagnetic compensation coefficients, 56th Ann. International Meeting: Society of Exploration Geophysics, Session:GM1.1.
- McDonald, J.R. and H.H. Nelson, 1998, MTADS Live Site Demonstration at Pueblo of Isleta, N.M., Report no. NRL/PU/6110-00-398.
- Nelson, H.H. and J.R. McDonald, 1999, Target shape classification using the MTADS: UXO/Countermines Forum 1999 Proceedings, Alexandria, Virginia, on CD-ROM.
- ORNL, 2004, Final Report on 2002 Airborne Geophysical Survey at Pueblo of Laguna Bombing Targets, New Mexico: ESTCP Final Report.
- Van, G.P., G. Calvert, L.P. Beard, T.J. Gamey, and A. M. Emond, 2004, Validation of Helicopter-Based Magnetic Survey at the Former Badlands Bombing Range: Expanded abstract in Proceedings of the Sixth Monterey Demining Symposium (MINWARA).

## 8 Points of Contact

Points of contact are given below in Table 8.1.

Table 8-1: Points of Contact

<b>Name</b>	<b>Organization</b>	<b>Phone</b>	<b>Project Role</b>
Gary Jacobs	ORNL	865-574-7374	Division Director
David Bell	ORNL	865-574-2855	Project Manager
Bill Doll	ORNL	865-576-9930	Technical Manager
Jeff Gamey	ORNL	865-574-6316	Operations Manager
Les Beard	ORNL	865-576-4646	Geophysicist
Scott Millhouse	USAESCH	256-895-1607	Project Lead
Jim Piatt	Pueblo of Isleta	505-869-5748	Environment Department Director
Barbara Bernacik	Pueblo of Laguna	505-552-7534	Environment Department Oversight
Emma Featherman-Sam	Oglala Sioux Nation	605-867-1271	Director, Badlands Bombing Range Project
Dan Munro	National Helicopters	905-893-2727	Helicopter Contractor President

## **Appendix A: Analytical Methods Supporting the Experimental Design**

None

## **Appendix B: Analytical Methods Supporting the Sampling Plan**

None

## **Appendix C: Quality Assurance Project Plan (QAPP)**

At the time of this survey, we were not required to have a QAPP in place, nor had ESTCP published the current guidelines for QAPP documentation (ESTCP Final Report Guidance for UXO Projects, Revision 2, April 2002). We nevertheless developed our own QA/QC procedures that were followed through this and other projects. These fall into three main categories: operational QA/QC, system QA/QC, and data QA/QC.

Under the category of operational QA/QC:

- Site visit preliminary to survey to assess appropriateness of site for helicopter geophysical surveying;
- De-gaussing of helicopter rotor to decrease magnetic noise produced by this component;
- Review of GPS almanac to assess best times of the day for surveying;
- Emplacement of a calibration grid for daily system checks;
- A morning meeting to coordinate each day's activities;
- An evening meeting to review activities and safety issues.

Under the category of system QA/QC:

- Installation of booms under the supervision of the pilot and engineer, and subsequent double-checking of all mounts and bolts;
- Daily helicopter inspection and maintenance by pilot and engineer;
- Ground tests of system after installation (checks to determine if all magnetometers are operating and have been connected in the correct order, and an impulse test to determine the lag between magnetometers and fluxgate);
- An initial check flight after installation.

Under the category of data QA/QC:

- An extensive test flight to evaluate the effects of pitch, roll, and yaw on the magnetometers, from which we can calculate compensation coefficients, and to examine the high altitude noise levels of the magnetometers.
- Daily inspection of diurnal magnetic activity at a base station magnetometer;
- Visual inspection of all data;
- Daily plots of flight path and laser altitude;
- Adherence to the data processing flow, described in section 3.6.6;
- Daily production of digital magnetic maps;
- Archiving of all materials: flight logs, digital materials, and report.

## **Appendix D: Health and Safety Plan**

This document represents the health and safety plan applied to field operations in New Mexico. Details in the plans for BBR and APG will vary accordingly.

### **D.1 Aircraft Base of Operations**

Albuquerque International Sunport  
2200 Sunport Blvd. SE  
Albuquerque, N.M. 87106  
Fixed Base Operator: Cutter Flying Service, Inc.  
Phone: 505-842-4184

The base of operations for all aircraft activities was Albuquerque International Sunport. The aircraft were stored and some refueling activities will occur at this location. Other refueling activities will occur remotely through use of a fuel truck provided by National Helicopters, Inc. No direct aircraft support (e.g., housing, fuelling, etc.) is requested from the Department of Defense.

### **D.2 Communications**

Air-to-ground and ground-to-ground communications occurred using two-way VHF radios provided by ORNL and National Helicopters. Radios broadcasted at 118 - 135 MHz. All other communications were via cellular telephones.

### **D.3 Schedule Constraints and Crew Rest**

#### **D.3.1 Schedule Constraints**

During aviation missions, activities can occur that are uncontrollable by the survey team and cause a delay of data acquisition. These activities may result in missed data acquisition windows or the loss of entire days of data acquisition.

#### **D.3.2 Crew Rest**

Crew rest will follow the guidelines prescribed by FAA regulations. Restrictions are placed on both the pilot's in-air flight-time and duty-time.

#### D.4 Aircraft

Bell 206L Long Ranger III Helicopter  
Color scheme: White with midnight blue and  
light blue accents  
Serial Number: 45784  
Tail Number: C-FNHG

National Helicopters, Inc.  
11339 Albion Vaughn Road  
Kleinburg, Ontario, Canada  
Phone: 905-893-2727

#### D.5 Statement of Risks

Airborne geophysical surveys are designed to be conducted with minimal risk to personnel. Safe operation of the aircraft is the *direct responsibility* of the pilot, who will determine the minimum safe flight altitude and local weather conditions for safe flying on an ongoing basis. The mission was flown under all applicable Federal Regulations.

Most ground activities were limited to routine working conditions; however certain field activities will expose personnel to summer heat and prairie wildlife. Precautions against the heat include drinking plenty of water, using sunscreen, and taking breaks as needed. Precautions against the wildlife include wearing hiking (or similar) boots and minimization of exposure to that environment. In addition, the two-man rule was in effect for all on-site field activities.

For additional risk-related information, consult the Operational Emergency Response Plan contained in Appendix B of this document.

#### D.6 Emergency Notification

Emergency action plans are included in the Appendix of this document. In the event of an emergency, staff will first request assistance, then provide appropriate first aid measures until emergency assistance arrives. As soon as emergency assistance has been obtained, the following people were to be notified in sequence based on availability:

Mr. David Bell, ORNL Project Manager

Cellular: 865-250-0578

Office: 865-574-2855

Dr. Bill Doll, ORNL Technical Manager

Cellular: 865-599-0820

Office: 865-576-9930

Mr. Jeff Gamey, ORNL Operations Manager

Cellular: 865-599-0820

Office: 865-574-6316

Mr. Scott Millhouse, USAESCH Program Manager

Office: 256-895-1607

Mr. Dan Munro, National Helicopter, President

Office: 905-893-2727

Dr. Steve Hildebrand, ORNL Environmental Sciences Division Director

Office: 865-574-7374

Home: 865-966-6333

**Each organizational member of the project team is responsible for flow-down of communications within the respective organization in the event of an incident or emergency** (e.g. notification of next-of-kin by ORNL Environmental Sciences Division Director if ORNL staff is involved in an emergency situation, etc.). Any member of the project team, in the event of an emergency situation, shall **not** contact persons other than those designated in the above listing.

#### **D.7 On-Site Ground Emergencies**

In the event of an emergency that occurs on-site:

- 1) Telephone local emergency response organizations via 911, if needed.
- 2) Conduct appropriate first aid.
- 3) Notify managers, as listed above in sequence. **The ORNL Project Manager has jurisdiction for all on-site emergency activities.** If the ORNL Project Manager is not available, the ORNL Technical Manager has jurisdiction.
- 4) The pilot has jurisdiction for emergency response when the aircraft is airborne, has crashed (if able), or has an emergency situation on the ground.
- 5) In the event of a catastrophic accident, the ORNL Environmental Sciences Division Director shall be notified immediately, and included in all response team activities, including communication, emergency response, and reporting.

#### **D.8 Off-Site Ground Emergencies**

In the event of an emergency that occurs off-site:

- 1) Assess the urgency of the emergency.
- 2) Telephone local emergency response organizations via 911, if needed.
- 3) Conduct appropriate first aid while awaiting professional assistance.
- 4) Notify managers, as listed above in sequence. **The ORNL Project Manager has jurisdiction for all off-site emergency activities.** If the ORNL Project Manager is not available, the ORNL Technical Manager has jurisdiction.

- 5) The pilot has jurisdiction for emergency response when the aircraft is airborne, has crashed (if able), or has an emergency situation on the ground.
- 6) In the event of a catastrophic accident, the ORNL Environmental Sciences Division Director shall be notified immediately, and included in all response team activities, including communication, emergency response, and reporting.

#### **D.9 In-Air Emergencies**

In-air emergencies were to be handled via standard aircraft emergency protocol, including radio contact with the Rapid City Regional Airport. **The pilot has jurisdiction for all emergency response activities and requirements when the aircraft is airborne.** Follow-up telephone/radio notification to the emergency response personnel listed in Section 11.0 were to be made as soon as possible.

## Appendix E: Dig list for APG from vertical gradient data

/Pick list from APG Airfield using ORAGS-VGrad data

/XY are in local coordinates (meters)

/AS is analytic signal peak in nT/m

/

ID	Priority	X	Y	AS	comment
1	1.00	313.0	394.5	4.982	scrap iron
2	1.00	166.5	387.5	6.072	
3	1.00	281.0	295.5	15.967	105mm seed
4	1.00	310.0	430.0	3.367	
5	1.00	199.5	336.0	3.867	handle
6	1.00	324.0	437.5	17.810	drum scrap
7	1.00	285.5	386.0	3.290	welding rods
8	1.00	356.0	354.5	5.030	
9	1.00	320.5	390.5	4.661	105mm seed
10	1.00	327.5	329.0	4.702	wire
11	1.00	282.0	368.0	5.393	81mm seed
12	1.00	270.0	324.5	14.287	
13	1.00	191.0	303.0	1.400	
14	1.00	155.5	333.5	30.710	
15	1.00	283.5	348.5	31.641	105mm seed
16	1.00	266.5	344.5	23.411	105mm seed
17	1.00	403.0	462.5	7.551	
18	1.00	250.0	307.8	38.771	105mm seed
19	1.00	156.3	358.8	13.519	
20	1.00	315.5	298.0	13.664	105mm seed
21	1.00	138.5	363.5	28.221	
22	1.00	295.5	298.5	23.797	105mm seed
23	1.00	266.0	410.0	18.344	
24	1.00	277.5	311.5	26.492	105mm seed
25	1.00	325.0	364.5	19.491	105mm seed
26	1.00	302.5	345.0	3.038	
27	1.00	173.5	383.5	7.304	
28	1.00	251.0	422.5	9.939	
29	1.00	172.5	350.5	5.920	
30	1.00	389.5	462.5	8.969	
31	1.00	262.5	352.5	11.511	
32	1.00	373.0	456.0	6.432	
33	1.00	344.5	341.0	6.891	
34	1.00	140.0	368.5	11.374	
35	1.00	198.5	286.5	6.760	
36	1.00	215.0	295.5	8.864	81mm seed
37	1.00	314.5	429.5	9.757	
38	1.00	346.5	438.5	7.650	spring
39	1.00	412.0	376.5	1.721	
40	1.00	209.0	257.5	8.183	
41	1.00	157.5	392.0	1.516	
42	1.00	204.0	290.5	6.922	
43	1.00	205.0	298.0	2.670	
44	1.00	235.5	319.5	2.688	81mm seed
45	1.00	452.5	435.5	3.312	
46	1.00	245.0	290.5	3.039	60mm seed
47	1.00	171.5	388.5	2.638	
48	1.00	333.3	442.0	12.727	
49	1.00	295.0	344.0	6.107	

50	1.00	311.8	301.3	9.848	105mm seed
51	1.00	174.0	267.0	8.979	
52	2.00	239.0	307.5	7.765	105mm seed
53	2.00	292.0	311.5	25.524	
54	2.00	389.5	387.0	8.648	
55	2.00	161.5	337.5	10.788	
56	2.00	169.5	331.0	8.655	
57	2.00	303.5	305.0	25.462	105mm seed
58	2.00	177.0	382.0	10.338	
59	2.00	224.3	290.0	36.696	105mm seed
60	2.00	419.5	376.5	14.466	
61	2.00	194.8	266.0	26.061	60mm seed
62	2.00	194.5	319.0	4.073	
63	2.00	413.0	360.5	3.008	
64	2.00	299.0	380.5	27.219	
65	2.00	307.5	407.5	1.645	
66	2.00	284.0	280.5	4.339	
67	2.00	174.5	385.0	7.814	
68	2.00	184.5	259.5	2.529	
69	2.00	437.5	381.5	6.262	
70	2.00	319.0	420.5	2.025	
71	2.00	156.5	363.0	5.823	
72	2.00	291.8	328.5	30.658	105mm seed
73	2.00	339.5	351.5	1.562	
74	2.00	219.0	306.8	11.312	105mm seed
75	2.00	319.5	358.0	6.850	81mm seed
76	2.00	287.5	337.5	37.464	105mm seed
77	2.00	327.5	442.5	11.666	
78	2.00	238.5	345.0	10.212	
79	2.00	447.5	457.5	7.698	
80	2.00	287.5	337.5	37.464	
81	2.00	333.0	432.0	7.510	
82	2.00	160.0	371.0	7.334	
83	2.00	265.0	328.0	22.570	105mm seed
84	2.00	262.5	365.0	29.503	
85	2.00	171.0	353.5	7.747	
86	2.00	296.0	436.5	12.341	
87	2.00	423.0	377.5	9.565	
88	2.00	283.0	427.0	10.450	
89	2.00	171.0	273.0	6.767	
90	2.00	168.5	316.0	9.449	
91	2.00	236.0	295.0	12.403	81mm seed
92	2.00	180.0	344.0	7.078	
93	2.00	269.5	325.0	15.940	105mm seed
94	2.00	322.5	402.0	1.624	
95	2.00	292.0	403.5	4.888	volcano mines
96	2.00	337.5	397.5	4.002	
97	2.00	289.5	397.0	2.574	
98	2.00	346.5	369.5	1.498	
99	2.00	167.5	270.0	5.463	
100	2.00	408.0	421.5	2.859	
101	2.00	341.5	386.5	2.852	
102	2.00	171.0	278.5	5.092	
103	2.00	406.5	410.0	1.342	
104	2.00	352.5	453.0	2.300	
105	2.00	237.5	353.0	1.246	scrap iron
106	2.00	415.0	349.0	5.129	

107	2.00	161.5	368.0	5.687	
108	2.00	404.0	457.0	1.302	
109	2.00	202.5	300.0	5.227	81mm seed
110	2.00	303.0	424.7	18.725	
111	2.00	293.0	421.0	1.430	
112	2.00	428.0	445.5	1.320	
113	2.00	417.0	446.0	4.729	
114	2.00	195.5	280.5	2.479	81mm seed
115	2.00	153.5	375.5	3.484	
116	2.00	346.0	337.0	2.558	
117	2.00	326.0	346.5	3.255	mower blade
118	2.00	276.0	317.5	3.171	81mm seed
119	2.00	267.5	303.5	2.315	81mm seed
120	2.00	320.5	388.0	4.129	
121	2.00	265.0	408.5	21.723	
122	2.00	289.0	360.0	3.714	81mm seed
123	2.00	216.0	346.0	1.353	flat stock
124	2.00	407.5	468.0	1.446	
125	2.00	430.0	403.0	4.973	
126	2.00	400.0	367.0	3.494	
127	2.00	266.8	408.5	20.162	
128	2.00	450.5	471.5	1.720	
129	2.00	271.0	305.5	1.765	
130	3.00	321.5	407.0	1.386	
131	3.00	273.5	305.0	1.491	
132	3.00	342.5	348.5	5.076	
133	3.00	192.0	313.0	1.631	
134	3.00	250.0	320.5	13.082	
135	3.00	301.0	395.0	1.280	
136	3.00	319.5	351.5	1.246	
137	3.00	240.5	345.5	9.867	
138	3.00	146.5	366.0	27.842	
139	3.00	284.0	295.5	24.906	
140	3.00	265.5	345.5	21.652	
141	3.00	183.0	354.0	22.767	
142	3.00	284.3	294.8	25.148	
143	3.00	402.0	375.0	1.331	
144	3.00	259.5	299.0	5.862	105mm seed
145	3.00	445.5	413.0	4.701	
146	3.00	234.3	296.8	18.343	
147	3.00	412.0	433.5	5.462	wire
148	3.00	172.0	321.0	5.462	
149	3.00	237.5	274.5	16.632	wire
150	3.00	352.0	441.0	1.435	
151	3.00	439.0	382.5	6.737	
152	3.00	159.5	274.5	1.414	
153	3.00	188.0	282.5	49.275	105mm seed
154	3.00	171.5	382.5	5.597	
155	3.00	283.0	428.5	12.749	
156	3.00	428.0	456.0	2.729	
157	3.00	311.5	423.0	1.327	
158	3.00	234.5	417.0	4.936	
159	3.00	323.5	335.0	3.259	81mm seed
160	3.00	391.0	387.5	7.733	
161	3.00	275.0	373.5	4.860	105mm seed
162	3.00	207.5	271.3	49.990	105mm seed
163	3.00	262.5	287.0	4.434	

164	3.00	266.5	326.5	10.400	81mm seed
165	3.00	342.5	385.5	2.901	
166	3.00	206.0	261.5	2.854	
167	3.00	358.0	363.5	1.216	
168	3.00	177.5	288.5	2.822	
169	3.00	213.0	291.5	3.495	
170	3.00	397.5	458.5	2.966	
171	3.00	300.0	379.5	19.344	
172	3.00	328.5	324.0	2.073	
173	3.00	401.5	344.5	3.519	
174	3.00	360.5	351.5	1.210	
175	3.00	157.5	383.5	2.586	
176	3.00	202.5	342.0	1.212	
177	3.00	255.5	401.0	49.087	wire
178	3.00	294.5	438.0	10.427	
179	3.00	364.0	456.5	2.451	
180	3.00	313.3	349.8	11.732	
181	3.00	261.0	283.5	11.100	bar stock
182	3.00	360.0	339.0	1.313	
183	3.00	175.3	259.5	16.854	
184	4.00	430.0	456.5	3.325	
185	4.00	303.0	406.5	1.212	
186	4.00	136.0	386.0	13.072	
187	4.00	176.5	260.0	15.771	
188	4.00	445.5	455.5	5.592	
189	4.00	226.5	406.0	1.277	
190	4.00	189.5	301.0	1.346	
191	4.00	145.5	387.5	4.869	
192	4.00	261.0	355.0	12.568	105mm seed
193	4.00	351.0	358.5	1.262	
194	4.00	322.5	397.5	1.314	
195	4.00	436.0	400.0	1.672	
196	4.00	183.5	357.5	43.513	
197	4.00	181.5	353.5	22.822	
198	4.00	265.5	320.5	4.088	pipe & ring
199	4.00	222.0	265.0	41.107	
200	4.00	199.5	354.5	1.380	
201	4.00	209.0	404.5	5.331	
202	4.00	331.5	330.0	1.325	
203	4.00	368.0	457.5	1.220	
204	4.00	353.0	344.0	1.306	
205	4.00	285.0	433.0	9.875	
206	4.00	162.0	386.0	1.940	
207	4.00	291.5	427.0	1.225	
208	4.00	257.0	401.5	42.980	
209	4.00	337.5	356.5	1.209	
210	4.00	289.5	297.5	48.866	
211	4.00	177.5	270.5	23.149	
212	4.00	198.0	366.0	1.726	
213	4.00	271.0	291.5	46.727	105mm seed
214	4.00	157.0	301.5	9.251	
215	4.00	370.5	363.0	3.613	
216	4.00	190.5	307.5	1.635	
217	4.00	152.0	382.5	3.123	
218	4.00	438.0	373.5	1.208	
219	4.00	192.5	318.0	3.317	
220	4.00	208.5	391.0	1.987	

221	5.00	334.0	327.5	1.329
222	5.00	220.0	265.5	33.650
223	5.00	200.5	259.5	1.285
224	5.00	267.5	276.0	13.972
225	5.00	165.0	300.0	5.013
226	5.00	244.5	318.5	42.965
227	5.00	451.3	449.0	35.319
228	5.00	427.5	460.0	1.350
229	5.00	288.0	297.0	38.952
230	5.00	216.3	379.3	42.045
231	5.00	286.5	296.5	26.758
232	5.00	194.0	282.5	2.610
233	5.00	151.0	357.0	23.784
234	5.00	261.8	362.8	43.973
235	5.00	159.0	377.0	3.039
236	5.00	260.5	291.0	1.344
237	5.00	205.0	287.5	9.594
238	5.00	390.0	401.0	1.379
239	5.00	417.5	354.0	1.245
240	5.00	168.0	378.0	7.741
241	5.00	199.0	380.0	1.229
242	5.00	288.5	296.0	26.145
243	5.00	164.5	288.5	8.489
244	5.00	191.0	327.0	1.990
245	5.00	337.5	331.5	1.203
246	5.00	300.5	291.5	1.367
247	5.00	343.0	326.0	1.388
248	5.00	149.5	383.5	3.082
249	5.00	310.0	399.0	1.286
250	5.00	339.0	427.0	4.709
251	5.00	260.5	292.5	1.395
252	5.00	353.5	362.0	1.265
253	5.00	197.5	314.0	1.428
254	5.00	168.0	352.0	4.943
255	5.00	149.0	351.0	15.617
256	5.00	185.0	361.5	10.037
257	5.00	191.5	269.0	9.613
258	6.00	342.5	322.0	1.399
259	6.00	187.5	368.5	20.238

105mm seed